

pubs.acs.org/JACS Article

# The Near-Sightedness of Many-Body Interactions in Anharmonic Vibrational Couplings

Ryan J. Spencer, \*\* Asylbek A. Zhanserkeev, \*\* Emily L. Yang, and Ryan P. Steele\*



Cite This: J. Am. Chem. Soc. 2024, 146, 15376-15392



**Read Online** 

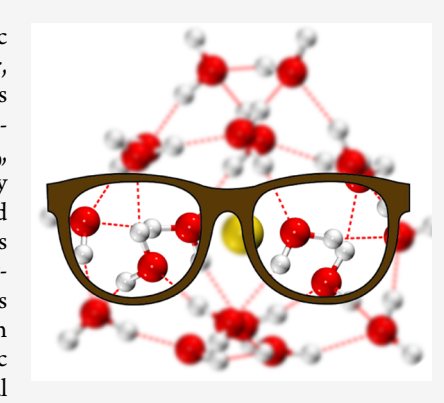
**ACCESS** 

Metrics & More

Article Recommendations

Supporting Information

**ABSTRACT:** Couplings between vibrational motions are driven by electronic interactions, and these couplings carry special significance in vibrational energy transfer, multidimensional spectroscopy experiments, and simulations of vibrational spectra. In this investigation, the many-body contributions to these couplings are analyzed computationally in the context of clathrate-like alkali metal cation hydrates, including  $Cs^+(H_2O)_{20}$ ,  $Rb^+(H_2O)_{20}$ , and  $K^+(H_2O)_{20}$ , using both analytic and quantum-chemistry potential energy surfaces. Although the harmonic spectra and one-dimensional anharmonic spectra depend strongly on these many-body interactions, the mode-pair couplings were, perhaps surprisingly, found to be dominated by one-body effects, even in cases of couplings to low-frequency modes that involved the motion of multiple water molecules. The origin of this effect was traced mainly to geometric distortion within water monomers and cancellation of many-body effects in differential couplings, and the effect was also shown to be agnostic to the identity of the ion. These outcomes provide new understanding of vibrational



couplings and suggest the possibility of improved computational methods for the simulation of infrared and Raman spectra.

### 1. INTRODUCTION

The characteristic vibrational motions of atoms serve as signatures for the identification of molecules and functional groups, as well as drivers of thermodynamic functions during chemical transformations.<sup>1</sup> The nuanced shifts in these frequencies reflect essential electronic-structure characteristics deriving from both covalent bonding and noncovalent interactions.<sup>2–20</sup> Infrared and Raman spectroscopies probe this vibrational behavior and, albeit indirectly, the potential energy and dipole/polarizability surfaces that govern vibrational dynamics. Couplings between vibrational motions serve as the physical mechanism by which heat and vibrational energy transfer occur, <sup>21–30</sup> and the same couplings—now probed by multidimensional spectroscopy experiments <sup>31–36</sup>— also serve as the dominant contributor to deviations from a canonical harmonic reference picture.<sup>37</sup>

Experimental advances in cold-ion sources and action spectroscopies have yielded considerable new insight into these vibrational dynamics, including the spectral signatures of ion hydration, hydrogen bonding, and biomolecular structure. Tolonomolecular structure. Because of the intrinsic need to "invert" such spectra into molecular structure and properties, theory and computational simulations have become vital partners in the interpretation of these modern experiments, \$9,37,38,40,46-57 particularly in the many cases that deviate strongly from a traditional harmonic analysis. A series of mature computational methods now exists for this purpose, including variational solvers 49-52,58 (on all or a targeted subset of vibrational modes) and more general methods that are often analogues of well-known methods in electronic structure theory. The

accuracy of these methods on relatively small chemical systems engenders considerable optimism for their ability to lend insight into the types of systems now accessed with modern experiments.

General usage of these approaches is hampered, however, by the practical need for nonlocal (or at least semilocal) representations of the vibrational potential energy surface (PES). Although "one-dimensional" anharmonicity—the deviation from the harmonic reference picture within a single vibrational mode—can sometimes be significant and likely forms the mental image of anharmonicity for many chemists, the multidimensional coupling between vibrational modes often serves as the dominant contribution to anharmonic spectra. It is also, unfortunately, the computational bottleneck for accurately modeling this anharmonic behavior. The ostensibly exponential scaling of such representations has limited these techniques to relatively small molecules/ complexes<sup>51,52</sup> or small subspaces of larger molecules.<sup>70</sup> The origin of this vibrational coupling is the central focus of the present study. Existing routes to alleviate this computational challenge include (1) new approaches to the numerical quadrature of the potential surface, 83-89 (2) the development

Received: March 4, 2024 Revised: May 1, 2024 Accepted: May 7, 2024 Published: May 21, 2024





of analytical representations of potential energy surfaces, 90-107 and (3) new physical insights into the nature of vibrational-coupling behavior. <sup>76,79,108–118</sup> The present analysis focuses on the latter approach, which has received relatively less attention but holds the potential to open entirely new avenues for the simulation and understanding of vibrational phenomena. The same analysis will exploit tools that have been provided by the second approach, however, including modern many-body potentials.

The many-body expansion is one of the oldest conceptual approaches in science, wherein the interaction between subunits of an n-component system is successively compounded in accuracy via one-body, two-body, ..., n-body terms and is typically truncated at some low order that is ideally long before n. In chemistry, such approaches have been used successfully to describe ion hydration, <sup>107,119–122</sup> molecular clusters, <sup>123–132</sup> and even biomolecules <sup>97,126,133–138</sup> and hydrocarbons. <sup>96,134</sup> This many-body framework is deployed in two ways in the present investigation, and it also serves to motivate the guiding questions. For clarity in nomenclature in the following analysis, n-mode terms will refer to a many-body expansion in vibrational modes, and n-body terms will refer to a many-body expansion of the potential energy surface in predetermined atomic/molecular fragments.

From the vibrational perspective, one of the standard routes to reducing the complexity of the governing PES is the "n-mode representation" (n-MR),  $^{54,61,63}$  which is effectively a many-body expansion in the space of vibrational modes (in selected vibrational coordinates,  $\{q\}$ , for an N-atom system of  $N_{\text{mode}} = 3N-6 \text{ vibrational modes}$ :

$$\begin{split} &V^{n\text{-MR}}(q_1,\,q_2,\,\cdots,\,q_{3N\text{-}6})\\ &=V_0+\sum_{i}^{N_{\text{mode}}}V^{(1)}(q_i)+\sum_{i}^{N_{\text{mode}}}\sum_{j>i}^{N_{\text{mode}}}\Delta V^{(2)}(q_i,\,q_j)\\ &+\sum_{i}^{N_{\text{mode}}}\sum_{j>i}^{N_{\text{mode}}}\sum_{k>j}^{N_{\text{mode}}}\Delta V^{(3)}(q_i,\,q_j,\,q_k)+\cdots \end{split} \tag{1}$$

In this expansion, the one-mode ("1-MR") terms are comprised of one-dimensional cuts along vibrational modes and capture the aforementioned 1D anharmonicity. Unfortunately, they are also often qualitatively incorrect—at least in rectilinear displacements—and often even yield the wrong sign of the anharmonicity. Instead, higher-order couplings, such as the pairwise couplings ("2-MR") of all modes in  $\Delta V^{(2)}$ , provide the necessary corrections that properly account for the strong anharmonicities and resonant effects that can qualitatively alter spectra from their harmonic reference. 9,37,139,140

Recent developments in analytic PES construction have taken a philosophically similar approach to potentials for water, hydrated ions, and some covalently linked systems:

$$V^{\text{MB}}(\vec{x}_{1}, \vec{x}_{2}, \dots, \vec{x}_{n})$$

$$= \sum_{i}^{n} V_{i}^{(1)}(\vec{x}_{i}) + \sum_{i}^{n} \sum_{j>i}^{n} \Delta V_{ij}^{(2)}(\vec{x}_{i}, \vec{x}_{j})$$

$$+ \sum_{i}^{n} \sum_{j>i}^{n} \sum_{k>j}^{n} \Delta V_{ijk}^{(3)}(\vec{x}_{i}, \vec{x}_{j}, \vec{x}_{k}) + \cdots$$
(2)

where each set of collective coordinates  $\vec{x}_i$  represents all degrees of freedom of fragment i. In this form, the incremental

energies, such as  $\Delta V_{ij}^{(2)} = V_{ij}^{(2)} - V_i^{(1)} - V_j^{(1)}$ , account for the differential electronic many-body effects that describe the mutual interaction of fragments. In the MBX (Many-Body eXpansion) representation 107 from Paesani, for example, predefined fragments (such as water molecules) exhibit their own intrinsic PES,  $V^{(1)\text{poly}}$ , using polynomial representations 102,104,141 fit to high-level quantum chemistry data. For the present ion hydrates, this reference quantum methodology was the coupled-cluster with singles, doubles, and perturbative triples [CCSD(T)] method, <sup>142</sup> combined with extrapolated cc-pwCVTZ-PP/cc-pwCVQZ-PP basis sets <sup>143</sup> for the alkali metal ions, along with their matched core potentials, 144 and the augcc-pVTZ/aug-cc-pVQZ basis sets<sup>145</sup> for oxygen and hydrogen atoms. Two-body terms include polynomial fits for short-range interactions,  $V^{(2)\text{poly}}$ , in addition to contributions from dispersion,  $V^{(2)\text{disp}}$ , via damped  $C_6$  interactions, and permanent electrostatics,  $V^{(2)\text{el}}$ . The three-body terms,  $V^{(3)\text{poly}}$ , similarly include polynomial fits to quantum chemistry data. Higherorder effects are captured via dipole polarization in a collective, induced-electrostatics correction  $V^{ef-pol}$ . The total potential is

$$\begin{split} V^{\text{MBX}}(\vec{x}_{1}, \, \vec{x}_{2}, \, \cdots, \, \vec{x}_{n}) \\ &= \sum_{i}^{n} V_{i}^{(1)\text{poly}}(\vec{x}_{i}) + \sum_{i}^{n} \sum_{j>i}^{n} \left[ \Delta V_{ij}^{(2)\text{poly}}(\vec{x}_{i}, \, \vec{x}_{j}) \right. \\ &+ \Delta V_{ij}^{(2)\text{disp}}(\vec{x}_{i}, \, \vec{x}_{j}) + \Delta V_{ij}^{(2)\text{el}}(\vec{x}_{i}, \, \vec{x}_{j}) \right] \\ &+ \sum_{i}^{n} \sum_{j>i}^{n} \sum_{k>j}^{n} \Delta V_{ijk}^{(3)\text{poly}}(\vec{x}_{i}, \, \vec{x}_{j}, \, \vec{x}_{k}) \\ &+ V^{\text{el-pol}}(\vec{x}_{1}, \, \vec{x}_{2}, \, \cdots, \, \vec{x}_{n}) \end{split} \tag{3}$$

Although the MBX potential's expansion truncates at this three-body term (with implicit higher-order effects stemming from dipole-polarization terms), more generic potentials, including those based directly on fragments computed from quantum chemistry computations, 121 -124,126-138,146-149 could also be included. Systematic analyses of these many-body quantum chemistry effects have shown that electronically insulating systems typically converge with three- to five-body terms, <sup>130</sup> depending on the types of interactions involved and the basis sets employed in calculations.

The clear formal similarity between these approaches naturally motivates the guiding questions of this investigation: namely, which many-body contributions in the PES contribute most significantly to the couplings that dictate vibrational anharmonicity? Are, for example, two-body terms in the underlying PES sufficient (or even necessary) to describe twomode coupling for anharmonic vibrations? Or alternatively, is the full, many-body potential required in order to describe these sometimes-subtle electronic-response effects? The answers to these questions hold considerable significance for computational simulation methods, two-dimensional vibrational spectroscopies, vibrational energy transfer, and the interpretation of infrared and Raman spectra.

This dual usage of the many-body expansion aligns in concept with the "double-incremental" approach of Christiansen and coworkers, 117,118 wherein FALCON-localized coordinates<sup>150</sup> have been employed to access linearly scaling anharmonic simulations of systems with well-defined fragments, including covalently linked systems. The present approach does not require or enforce strict localization of vibrational modes to the same fragments as the many-body potential method, although the selected localized coordinates often yield this outcome in practice for most of the modes. But this computational nuance aside, the present investigation complements this previous work by directly addressing the underlying physics of vibrational couplings and the reasons that a rapid convergence of the many-body expansion of the PES could still be obtained with multimode vibrational couplings.

Using hydrated-ion clusters as a first testing platform (Figure 1), this investigation addressed these questions using MBX and

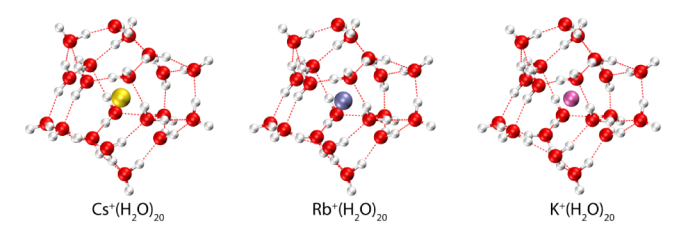


**Figure 1.** Optimized structures of hydrated-ion clusters considered in this work. All three clusters were optimized with the MBX potential.<sup>107</sup> The cesium starting structure was taken from ref 40, and the rubidium and potassium structures were relaxed upon ion substitution. All three structures maintain the known clathrate-like form of the cesium-containing cluster.

density functional theory (DFT) potentials. The main—and perhaps surprising—outcome is that, although all terms in the MBX potential are critical for describing harmonic frequencies and one-dimensional anharmonicity, only *one*-body terms contribute substantively to the anharmonic couplings between vibrational motions. These dominant one-body terms are also naturally short-ranged. From the outset, these conclusions must be tempered by the fact that they are tested on only a single class of chemical systems. Although we suspect that they are reasonably general, for reasons that will be discussed below, considerable future analysis on disparate chemical systems is encouraged.

## 2. METHODS

The aim of the present investigation was to assess the role of many-body contributions to anharmonic vibrational couplings. Accordingly, the approach to determining these roles was a straightforward decomposition of these couplings into their constituent many-body terms. In broad terms, anharmonic couplings were computed for a series of hydrated-ion test systems, and the contribution from each many-body component of the underlying PES was computed.

The chemical systems studied in this work included the clathrate-like, hydrated-ion cages of alkali metal cations. Specifically,  $Cs^+(H_2O)_{20}$ ,  $Rb^+(H_2O)_{20}$ , and  $K^+(H_2O)_{20}$  clusters were investigated as a convenient preliminary platform. The structure of  $Cs^+(H_2O)_{20}$  was taken from ref 40 and reoptimized with the potentials described below. The structures for the rubidium- and potassium-containing clusters were optimized using this cesium-containing structure as an initial guess, and they relaxed to a qualitatively identical clathrate-like structure, as shown in Figure 1. The resulting structures for these two ions are not guaranteed to be the global minimum but nonetheless provide a direct comparison of vibrational couplings as a function of ion identity.

Coordinates for all equilibrium structures are provided in Section S1 of the Supporting Information.

The MBX potential was employed for geometry, frequency, and PES scan calculations in this investigation. The potentials for these three ions were used with default settings, except for the removal of the one-body energy cutoff to account for large displacements during PES scans, using code obtained from GitHub. The MBX code was only modified to (a) print the relevant components of the total MBX energy, as partitioned in eq 3, and (b) optimize structures using specific components of the total MBX gradient for subsequent harmonic analyses. The MBX libraries were otherwise integrated as-is into parallelized, in-house code for performing the PES scans for anharmonic couplings.

The vibrational analysis consisted of computations of harmonic spectra, variational eigensolvers for one-dimensional anharmonic states, and 2-MR vibrational couplings. Harmonic spectra were computed in the traditional normal-mode picture, using structures that were first optimized for each combination of energy components to a tolerance of  $10^{-6}$  kcal mol<sup>-1</sup> Å<sup>-1</sup>. Hessians were computed via finite differences of analytic first derivatives of the MBX energies, using a step size of 10<sup>-5</sup> Å. For the harmonic spectra, only total dipole contributions were considered in this work since the many-body decomposition of dipole moments in MBX follows a different partitioning scheme. Thus, only the impact on frequencies, rather than intensities, was analyzed. Anharmonic couplings were limited to pairwise (2-MR) terms for the sake of isolating many-body contributions in this first analysis. This two-mode coupling approximation has been the most commonly employed approach for larger molecules<sup>70</sup> and is almost invariably the strongest coupling observed in molecular systems, although truncating the n-MR expansion at this order can sometimes lead to pathological potentials for large molecules and lowfrequency motions. 152 Nonetheless, it provides the most direct assessment of the role of many-body effects in vibrational anharmonicity. Only the values of these couplings were examined, and their overall role in the final spectrum has intentionally not been assessed, due to both the sensitivity of the latter effect to the choice of anharmonic simulation method (VSCF, VCI, etc.) and the pathological contribution of lowfrequency modes to the  $X^+(H_2O)_{20}$  spectra unless high-order n-MR potentials are employed. As a conceptual guide to the reader, however, we note that the magnitude of the anharmonic shift in a vibrational state energy by a single coupling matrix element would be bounded, from above, by the value of this coupling in a 2 × 2 mode-pair problem. Of course, the effect of these couplings could become additive (or cancel) in a multimode chemical system. Without a priori knowledge of the strength or origin of these couplings, however, the user would have no means to predict these shifts, hence the daunting computational challenge of anharmonic simulations. As a preliminary estimate of these effects, twodimensional anharmonic spectra for selected, strongly coupled mode pairs were computed by diagonalizing the (rotationless) vibrational Hamiltonian in the same harmonic basis set used for coupling integration.

Within the anharmonic analysis, integration over the 2-MR PES was performed with Gauss—Hermite quadrature <sup>153</sup> using 11 grid points (G). For pairwise couplings on the present ion—water clusters, these quadratures consist of  $\frac{N_{\text{mode}} \cdot (N_{\text{mode}} - 1)}{2}$   $G^2 = 1.88 \times 10^6$  PES evaluations. A harmonic-oscillator basis of 10

states, centered at equilibrium and with widths matched to the harmonic or local-mode pseudoharmonic 108,110 frequencies, as appropriate, was employed for integrating all coupling matrix elements. For most of the analysis, window-localized (500 cm<sup>-1</sup> window), rectilinear vibrational modes<sup>109</sup> were employed, using the simple Jacobi sweeps-based, unitary-rotation approach of refs 109 and 110. The full potential was used to determine local-mode displacements, regardless of the manybody term(s) used to perform the anharmonic PES quadrature. Although a root-mean-squared (RMS) definition of the integrated anharmonic coupling,  $\langle 00|(\Delta V^{(2)})^2|00\rangle^{1/2}$  (where state labels correspond to harmonic basis states and integration is performed over the two involved vibrational degrees of freedom), has been employed in previous local-mode analyses, 108,109,154 this approach posed two problems for the present investigation. First, it is an unsigned quantity that does not allow for an assessment of cancellation of component terms; second, the squared integrand would introduce crossterms between many-body components. For these reasons—in addition to the fact that the following alternative terms are the ones that actually enter anharmonic simulations—specific anharmonic-coupling matrix elements,  $C_{\nu\nu,\nu'\nu'_i} = \langle \nu_i \nu_j | \Delta V^{(2)}(q_i, q_i) | \nu'_i \nu'_j \rangle$ , were instead investigated. All matrix elements were computed, and a series of relevant coupling matrix elements will be discussed in the following analysis, as a function of both mode-pair distance and manybody truncation order.

Finally, to confirm that the qualitative conclusions of this analysis were not limited to MBX-type many-body potentials, a series of representative mode-pair couplings was reanalyzed with density functional theory (DFT) potentials for  $Cs^+(H_2O)_{20}$ . After assessing a series of functionals for congruence with MBX harmonic spectra, the B97M-V functional <sup>155</sup> was employed and paired with the pruned SG-3 electronic quadrature grid. <sup>156</sup> The cc-pVDZ basis set was used for oxygen and hydrogen atoms; the cc-pVDZ-PP basis set (obtained from ccRepo <sup>157</sup>) and matched ECP46MDF core potential were used for the cesium atom. All supersystem and fragment computations were performed in the Q-Chem quantum chemistry software package, <sup>158</sup> and many-body decomposition of the total cluster was performed with inhouse code to generate the fragment calculations at each quadrature point.

## 3. RESULTS AND DISCUSSION

As spectroscopic reference points and to set the scale for the anharmonic-coupling analysis that follows, harmonic and 1D anharmonic spectra are first presented. Analysis of mode-pair couplings will follow thereafter.

**3.1. Harmonic Spectra.** The normal-mode, unscaled, harmonic spectra for  $Cs^+(H_2O)_{20}$  are depicted in Figure 2. The total MBX spectrum [2(a)] consists of the expected bands of symmetric and antisymmetric O–H stretches (3238–3828 cm<sup>-1</sup>); H–O–H bends (1665–1739 cm<sup>-1</sup>); and a series of low-frequency, heavy-atom, and librational motions (26–1026 cm<sup>-1</sup>). The one-body spectrum [2(d)] is, by construction, solely comprised of 20 identical water-monomer spectra and excludes this low-frequency response as well as all bilinear interactions between high-frequency motions. The two-body MBX terms lead to substantial perturbations to the harmonic spectrum [2(c)], including shifts in the O–H stretch region, modest splitting of the water bends, and the appearance of the

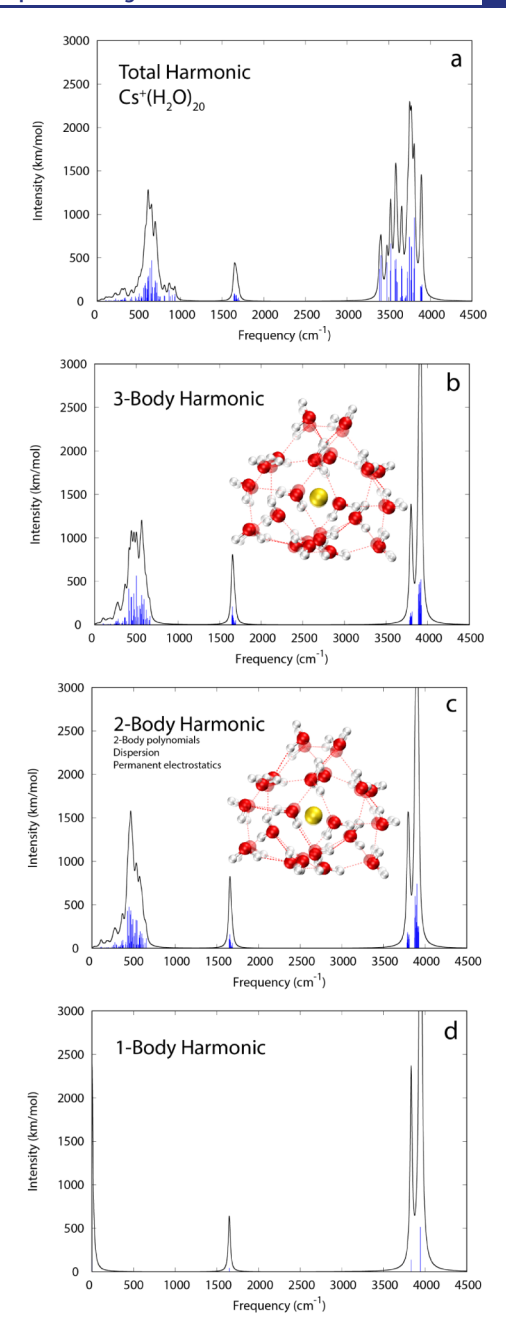


Figure 2. Harmonic infrared absorption spectra of  $Cs^+(H_2O)_{20}$ , computed with the (a) total potential, (b) summed one-, two-, and three-body potentials, (c) summed one- and two-body potentials (including polynomials, dispersion, and permanent electrostatics), and (d) one-body potentials. Spectra for the lower three panels were computed at structures reoptimized with the accordant forces, using the total potential's structure as the starting guess. The inset in the middle panels overlays the many-body structure (solid) with the total potential's structure (translucent) for comparison. (The two structures were first aligned by minimizing their mutual RMSD via rigid translations and rotations.) In each panel, blue stick spectra are depicted along with a summed spectrum from a 30 cm $^{-1}$  Lorentzian broadening in solid black lines.

entire spectral response below 1000 cm<sup>-1</sup>. After alignment of mode displacements, the root-mean-squared deviation (RMSD) between one- and two-body harmonic spectra was computed to be 265.8 cm<sup>-1</sup>, with a modest 35.0 cm<sup>-1</sup> shift in just the water bends and stretches. The maximum shift was

651.1 cm<sup>-1</sup>, corresponding to the activation of a collective water wagging/rocking motion upon inclusion of two-body terms. Additional shifts of 7.7 and 6.4 cm<sup>-1</sup> (RMS) in the total and bend/stretch regions, respectively, were observed upon inclusion of three-body MBX terms. The maximum change of -24.9 cm<sup>-1</sup> corresponds to a red-shift in a collective, waterwagging motion. Crucially, the induced-electrostatic terms engender considerable spectral alteration, particularly in the O-H stretching region. Evidently, polarization's contribution to hydrogen-bonded O-H stretch frequencies is critical, at least within this partitioning of the potential. These induced electrostatics recover the remnant 120.0 cm<sup>-1</sup> error (124.8 cm<sup>-1</sup> in the bends and stretches) that persists in the threebody spectrum. The maximum shift of -425.8 cm<sup>-1</sup> occurs in a hydrogen-bonded O-H stretching mode. This result is perhaps intuitive, given the known, partially covalent character of hydrogen bonds. 159 This outcome is nonetheless instructive since this spectral shift is captured by the induced electrostatics, rather than the short-ranged two- and three-body polynomials alone. Therefore, the full MBX potential is evidently necessary for a correct depiction of the  $Cs^+(H_2O)_{20}$  harmonic vibrational spectra.

As shown in Figures S1–S3, the harmonic spectra exhibit nontrivial shifts when the identity of the ion is changed, although the qualitative spectral response is similar among the ions. Due to both vibrational Stark shifts 160–162 and contraction of the hydrogen-bonding network based on the size and charge density of the ion, all regions of these spectra exhibit spectroscopically relevant frequency shifts. Most relevant to the present analysis, however, is the observation that the many-body contributions to these alternative spectra remain significant for all ions.

**3.2. 1D Anharmonic Shifts.** By constructing and diagonalizing the (rotationless) vibrational Hamiltonian in the basis of harmonic oscillator states for each of the 177 vibrational modes in the ion-hydrate clusters, the 1D anharmonicity of each mode was assessed. Results are presented in Figure 3 for the fundamentals ( $\nu = 0 \rightarrow \nu = 1$ )

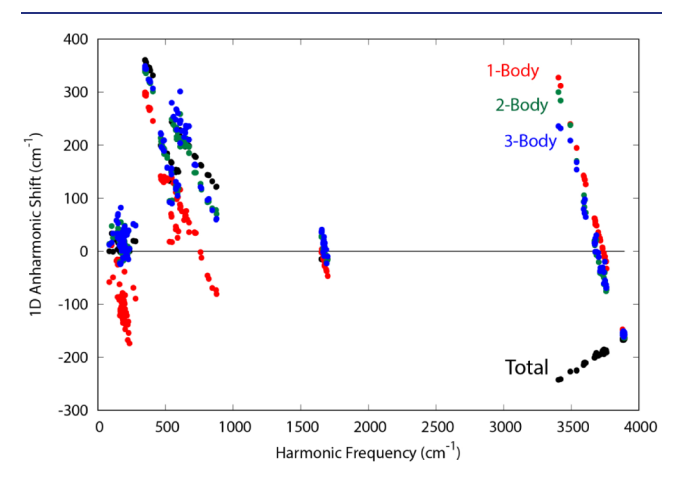


**Figure 3.** Many-body decomposition of 1-MR anharmonic shifts for all window-localized vibrational modes in  $Cs^+(H_2O)_{20}$ . The anharmonic shifts are defined relative to the harmonic pseudofrequencies of the localized modes. The two-body terms include two-body polynomials, dispersion, and permanent-electrostatic contributions. Results for two-body and higher methods include the summed contributions from preceding terms. The "Total" values include induced-electrostatics contributions.

in Cs<sup>+</sup>(H<sub>2</sub>O)<sub>20</sub>. The RMS anharmonic shift (black data points in Figure 3), relative to the local-mode, harmonic pseudofrequencies, was 159.9 cm<sup>-1</sup> or 17.8% of the harmonic value. These total shifts were mainly to the blue for low-frequency modes and to the red for the water bends and stretches. (This behavior is already an improvement due to localized modes, as the sign of the 1D anharmonic shift in the antisymmetric stretch of an isolated water molecule is typically incorrect in normal modes.) Not surprisingly, the results for pure one-body potentials (red data points) are qualitatively in error, just as was the case for their harmonic counterparts. Without the twobody and higher interactions, these 1D, one-body potentials correspond simply to various cuts along the potentials of isolated water molecules. Thus, the one-body anharmonic results are in error (RMS) by 155.1 cm<sup>-1</sup>, which is nearly as large as the anharmonic shift itself. Just as was observed with the harmonic spectra, the two-body (green data points) and three-body (blue data points) terms make meaningful but modest contributions to the 1D anharmonicity, reducing the RMS errors to 111.8 and 108.9 cm<sup>-1</sup>, respectively. The induced-electrostatic terms are clearly critical here and account for this extant error, which comprises more than two-thirds of the overall error. For many of the O-H stretching modes particularly the hydrogen-bonded stretches—these inducedelectrostatic contributions change the sign of the anharmonicity, and the RMS shift due to induced electrostatics in this O-H stretch region is 222.8 cm<sup>-1</sup>. Evidently, all of the manybody terms are required for even a qualitatively correct description of this diagonal anharmonicity. The polynomial three-body terms are least impactful, at least in the partitioning considered in this subsection, and the induced-electrostatic terms perform the proverbial lion's share of the work in describing these anharmonic effects.

The cation plays a nontrivial role in altering these 1-MR anharmonic shifts; analogous results for  $Rb^+(H_2O)_{20}$  and  $K^{+}(H_{2}O)_{20}$  are depicted in Figure S4. The contraction of the water network in the vicinity of the more compact and chargedense ions leads to an increase in the magnitude of the anharmonic shifts in the O-H stretching modes. The overall RMS shifts are reduced to 158.9 cm<sup>-1</sup> for Rb<sup>+</sup> and 122.6 cm<sup>-1</sup> for K+, but these values are strongly impacted by the water bending motions and motions at lower frequencies. In the O-H stretch region, these RMS shifts remain 200.0 and 120.1 cm<sup>-1</sup> for the two ions. The need remains for all many-body terms, however, including the dominant role of induced electrostatics. These latter terms account for 114.4 cm<sup>-1</sup> (Rb<sup>+</sup>) and 165.4 cm<sup>-1</sup> (K<sup>+</sup>) of the total RMS shifts. Although the polarizability of the ion decreases across the {Cs+,Rb+,K+} series, evidently the ion's role in polarizing the surrounding water network increases across the same series and leads to increased contributions of polarization to the 1-MR anharmonicities.

**3.3. Many-Body Anharmonic Couplings.** The outcome for anharmonic couplings was found to be decidedly different than their harmonic and one-mode counterparts, however. The many-body contributions to pairwise,  $C_{00,00}$  couplings (i.e., the direct shifts in the zero-point state) in  $Cs^+(H_2O)_{20}$  are depicted in Figure 4. Each panel compares the total pairwise, local-mode vibrational coupling to the same quantity computed from many-body contributions from the MBX potential. The main outcome of this work is shown in Figure 4a: The two-mode vibrational coupling is almost entirely dictated by *one-body* terms in the many-body potential.

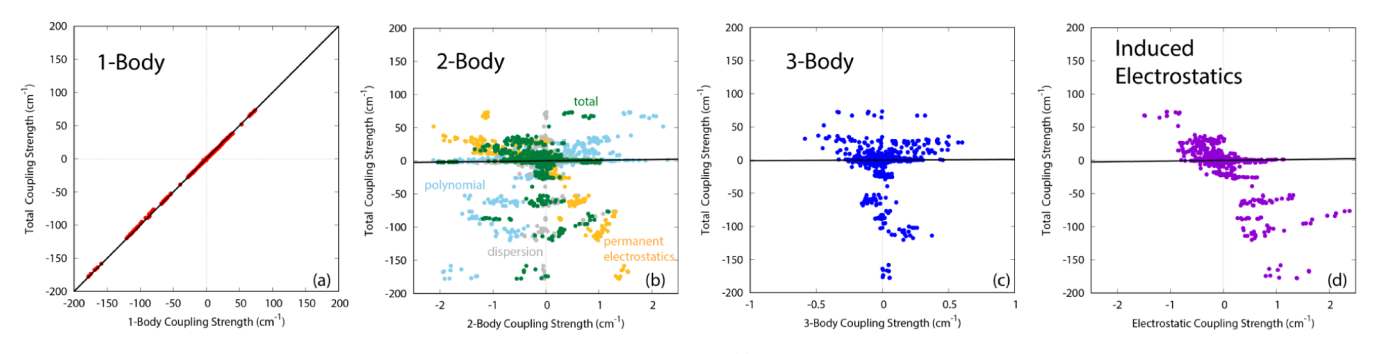


Figure 4. Many-body decomposition of anharmonic couplings,  $C_{00,00} = \langle 00|\Delta V^{(2)}(q_p,q_j)|00\rangle$ , for all unique pairs of vibrational modes in Cs<sup>+</sup>(H<sub>2</sub>O)<sub>20</sub>. The black diagonal line in each panel corresponds to y=x as a visual guide and is not a fit to the data. The two-body terms in panel (b) include short-range polynomial fits, two-body dispersion, and permanent electrostatics; the summed couplings from these terms are also depicted. Panel (d) depicts only contributions from induced electrostatics.

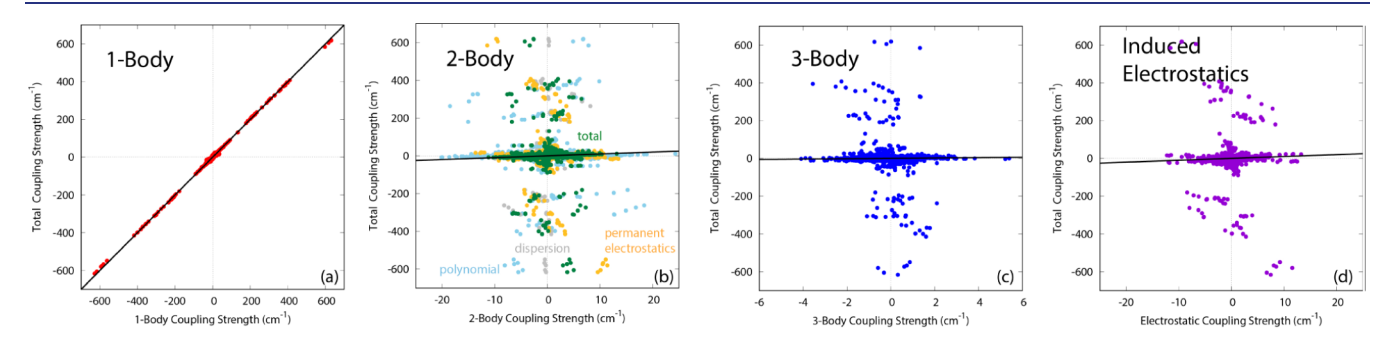


Figure 5. Many-body decomposition of anharmonic couplings,  $C_{00,01} = \langle 00|\Delta V^{(2)}(q_\nu q_j)|01\rangle$  and  $C_{00,10}$ , for all unique pairs of vibrational modes in  $Cs^+(H_2O)_{20}$ . The black diagonal line in each panel corresponds to y=x as a visual guide and is not a fit to the data. The two-body terms in panel (b) include short-range polynomial fits, two-body dispersion, and permanent electrostatics; the summed couplings from these terms are also depicted. Panel (d) depicts only contributions from induced electrostatics.

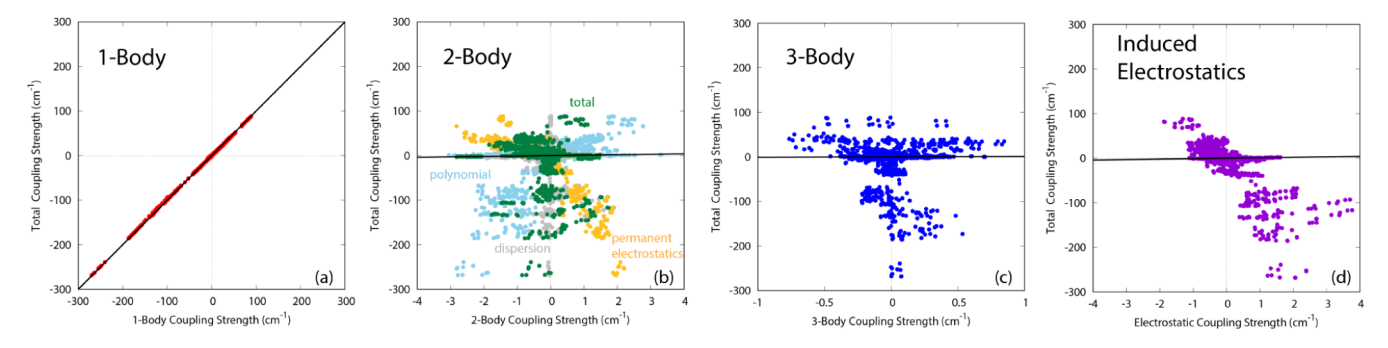


Figure 6. Many-body decomposition of anharmonic couplings,  $C_{00,02} = \langle 00|\Delta V^{(2)}(q_pq_j)|02\rangle$  and  $C_{00,20}$ , for all unique pairs of vibrational modes in  $Cs^+(H_2O)_{20}$ . The black diagonal line in each panel corresponds to y=x as a visual guide and is not a fit to the data. The two-body terms in panel (b) include short-range polynomial fits, two-body dispersion, and permanent electrostatics; the summed couplings from these terms are also depicted. Panel (d) depicts only contributions from induced electrostatics.

Although some nonzero two- and three-body contributions exist, they are invariably small and show little systematic correlation with the total coupling. [The horizontal axes are contracted, by  $80\times$  and  $200\times$ , respectively, in Figure 4b–d. A version of the same figure with full axes is provided in Figure S5.] For total couplings with magnitudes  $\geq$ 5 cm<sup>-1</sup>, the one-body terms comprise an average of 102% of the magnitude of the total coupling; total two-body terms comprise 1.6%; three-body and induced-electrostatic terms contribute a mere 0.6% and 1.6%, respectively, to the total coupling within this ion hydrate for this matrix element. Some of the polynomial two-body terms show some modest correlation with the total coupling, indicating that at least some slight cross-monomer communication influences the anharmonic couplings, but they

are uniformly small in magnitude. Furthermore, the permanent (and induced) electrostatic terms exhibit behavior that partially offsets this short-ranged two-body coupling, reducing the total two-body coupling further. The three-body terms were found to be even smaller (ranging only approximately  $\pm 0.5~{\rm cm}^{-1}$ ) and exhibit essentially no correlation with total coupling values. Anecdotally, we note that some matrix elements were observed to exhibit a large fractional two-body (or higher) contribution, but these cases were invariably quite small elements that have little impact on overall anharmonicity.

Other matrix elements exhibited very similar behavior, as shown in Figures 5 and 6; data corresponding to additional matrix elements can be found in Figure S6. For the  $C_{00,01}$  and  $C_{00,10}$  elements (Figure 5) that could also shift the ground-state

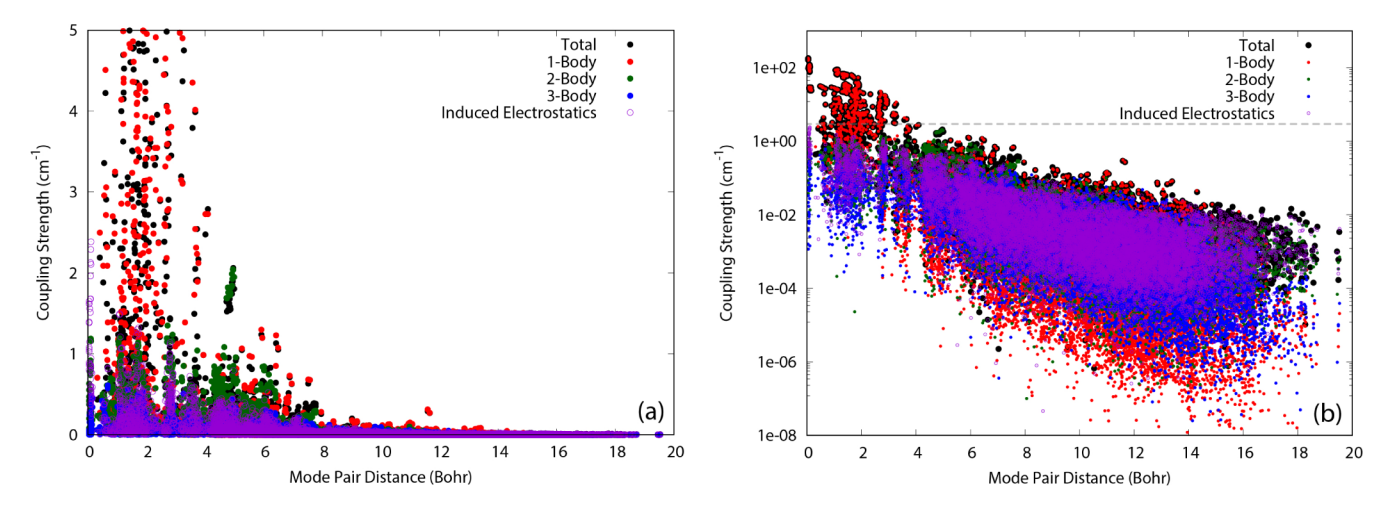


Figure 7. Distance dependence of anharmonic couplings,  $C_{00,00}$ , for all unique pairs of vibrational modes in  $Cs^+(H_2O)_{20}$ . The same data are plotted in both panels. The left panel shows a contracted vertical axis, allowing an assessment of the long-distance tail of the coupling components. The right panel shows the full, logarithmic vertical axis. The dotted line in the right panel corresponds to a coupling value of 3.0 cm<sup>-1</sup>.

and fundamental energies, for example, the one-body dominance was once again observed, even for matrix elements that span approximately three times the coupling magnitude as  $C_{00.00}$ . Some slight one-body deviation from the total coupling values was observed for this matrix element for small coupling values (near the origin in Figure 5a), but the RMS deviation between one-body and total couplings was only 1.0 cm<sup>-1</sup> across this singly excited set of elements. In this case, the twobody contributions were observed to be somewhat larger in absolute magnitude but remained fractionally small. The polynomial and permanent-electrostatic pieces were again found to partially cancel. The qualitative outcomes were nearly identical for the  $C_{00,02}$  and  $C_{00,20}$  elements depicted in Figure 6, for total coupling values that sit intermediate to those of  $C_{00,00}$ and  $C_{00,01}/C_{00,10}$ . Indeed, across the set of all potential matrix elements  $C_{\nu_i \nu_i, \nu_i' \nu_i'}$ , the behavior was found to be almost uniformly similar. This transferability, as shown in Figure S6, provides reasonable confidence that the total coupling engendered between, for example, anharmonic states, would also be one-body-dominant.

The lone exception to this trend was the set of  $C_{00,11}$ -type coupling terms and all other elements where the coupled states both changed by a single quantum of excitation,  $C_{\nu_i\nu_j,\nu_i+1\nu_j+1}$ . In this case, additional spread in the one-body terms was observed, as depicted in Figure S7. Upon reflection, this outcome should reasonably have been anticipated for localized modes and is not indicative of new behavior for this lone class of anharmonic coupling. In rectilinear, localized vibrational modes, the mass-weighted Hessian is no longer diagonal,  $^{108,110}$  yielding off-diagonal terms that would correspond to bilinear coupling operators  $\frac{\partial^2 V}{\partial q_i \partial q_i} q_i q_j$  in a Taylor representation of the

PES. Local modes trade this low-order coupling for predictable distance-decay behavior. In the present case, these couplings are dominated by pseudoharmonic (bilinear) contributions. Because the harmonic potentials were already shown to require all many-body terms in Section 3.1, their significant role in these bilinear couplings follows logically. Importantly, these terms can be integrated analytically (and existing methods to account for this "harmonic correlation" exist<sup>163</sup>) and can be separated easily from the true anharmonic contributions,

leaving behind many-body trends that are once again analogous to those for all of the other vibrational coupling terms.

The ion dependence of this behavior is shown in Figures S8 and S9 for  $Rb^+(H_2O)_{20}$  and  $K^+(H_2O)_{20}$ , respectively. The overall trends for the  $C_{00,00}$  anharmonic coupling are unchanged for these ions. The spread in the coupling values for total two-body and polarization contributions marginally increases as the ion becomes more compact; the dominance of the one-body terms remains intact. The maximum contribution from the induced electrostatics, for example, is 2.39 cm<sup>-1</sup>, 2.62 cm<sup>-1</sup>, and 2.76 cm<sup>-1</sup>, respectively, for Cs<sup>+</sup>, Rb<sup>+</sup>, and K<sup>+</sup>. All three of these values correspond to couplings involving a localized O-H stretch that donates a hydrogen bond and the wag motion of the same O-H bond. The smaller size of the cation leads to slightly stronger hydrogen bonding and marginally more contribution to anharmonicity from the induced electrostatics. These effects, which were shown to be large for harmonic and 1D anharmonic spectra, are clearly quite small in the anharmonic couplings, even though the total anharmonic coupling values span ≈250 cm<sup>-1</sup> for this matrix

The distance-decay behavior of the coupling terms was also examined, and results are depicted in Figure 7 for  $C_{00,00}$ . A magnified version of the long-distance tail of these patterns is first shown in Figure 7a and is generally consistent with the local-mode distance dependence observed in previous analyses. 108,109,154 At this scale, the long-distance behavior of one-, (total) two-, three-body, and induced-electrostatic terms appears to be approximately equal and does not necessarily suggest the origin of the behavior observed in Figures 4-6. In Figure 7b, the same data are instead plotted on a logarithmic vertical axis, with a scale now showing all  $C_{00,00}$  couplings. This alternative presentation highlights several attributes. First, an incredible number of local-mode, pairwise couplings exist at small values (below a few cm<sup>-1</sup>); this attribute is not necessarily obvious in the linear-axis plots. Second, the general slopes of the component coupling distributions differ slightly (although they contain sufficient spread-4 to 10 orders of magnitude—that linear fits are likely not meaningful), indicating that they do exhibit slightly different distancedecay behavior. Third, and most relevant to the present

questions, the strong-coupling region is once again almost entirely dominated by one-body contributions, as indicated by the dotted line at an arbitrarily chosen 3 cm<sup>-1</sup> cutoff in Figure 7b. Only short-range (<4 Bohr), one-body couplings are necessary in order to capture the entirety of this strongcoupling region. The few two-body contributions that approach this cutoff also exist only at short distances, suggesting that established approaches for distance-based truncations of local modes could perhaps be employed if remnant two-body contributions are necessary. Interestingly, a small handful of three-body and induced-electrostatic contributions also approach this strong-coupling cutoff, but these terms only appear at near-zero mode-pair distances. Evidently, these nominally many-body terms paradoxically lead to some slight and indirect intramonomer mode coupling. Whether these very short-range effects can be exploited by modified (and, presumably, accelerated) three-body and inducedelectrostatic approaches remains an open question for future investigation.

**3.4.** Source of Many-Body Behavior and Coupling Examples. The obvious question posed by this perhaps-surprising outcome is why this one-body dominance might occur. How is it possible, for example, that pairs of vibrational modes—which clearly involve communication across hydrogen-bonded monomers at the harmonic level—could have their anharmonic couplings be almost entirely described by one-body terms in a many-body potential? To answer this question, three representative mode pairs, the local-mode displacements of which are depicted in Figure 8 and labeled A/B/C, were examined and will be discussed in turn in this section. Due to the intrinsic limitations of representing molecular motion in static images, animations of the same mode displacements can also be found in Section S5. The component coupling contributions are listed in Table 1.

The mode pair (A) with the strongest observed groundbasis-state coupling ( $C_{00,00} = -177.7 \text{ cm}^{-1}$ ) involves a dangling O-H stretch mode and wagging mode of the same water molecule. These two motions exhibit pseudoharmonic localmode frequencies of 3894 and 348 cm<sup>-1</sup>, respectively. The rectilinear displacement of this low-frequency wag motion would lead to elongation of the O-H bond, and contraction of this coordinate via the localized O-H stretch is necessary in order to generate approximately rigid-body motion of this water molecule. (Such coupling would likely be much smaller in curvilinear coordinate systems. 164-169) The one-body nature of this coupling is obvious for this particular mode pair since the two motions are localized to the same water molecule, and the window-localized modes yield little motion of the remaining atoms. Indeed, the one-body coupling for this pair is -178.6 cm<sup>-1</sup>, which only overestimates the total coupling by 0.5%. Evidently neither the O-H stretch nor the rocking reorientation of this single-water motion is sufficiently perturbed by the two-, three-, or many-body MBX terms to strongly impact the anharmonic coupling. The total two-body contribution is only -0.55 cm<sup>-1</sup>, which is comprised of -1.92cm<sup>-1</sup> from the short-range, polynomial fit terms, -0.03 cm<sup>-1</sup> from dispersion terms, and 1.39 cm<sup>-1</sup> from permanentelectrostatic terms. Thus, some cancellation of contributions is partly responsible for the overall small magnitude of the twobody coupling, but these constituent pieces also remain quite small. Even though the induced electrostatics played a prominent role in the harmonic and 1-MR anharmonicities,

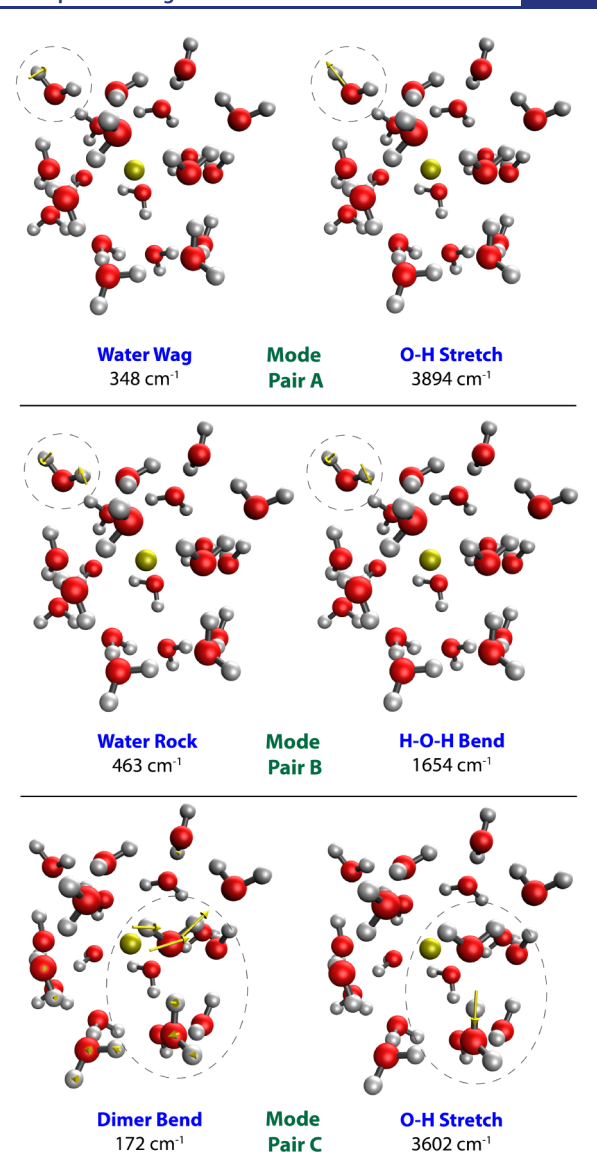


**Figure 8.** Three representative, strongly coupled mode pairs in  $Cs^+(H_2O)_{20}$ . Shown are the local-mode displacements, represented by yellow arrows that are superimposed on the equilibrium structure. Harmonic pseudofrequencies are also listed for each mode. As a guide to the eye, dotted lines encircle areas of significant molecular motion.

Table 1. Many-Body Contributions to Two-Mode Anharmonic Couplings (cm<sup>-1</sup>) for Cs<sup>+</sup>(H<sub>2</sub>O)<sub>20</sub> Mode Pairs Depicted in Figure 8, Using the MBX Potential

|                          | mode pair |       |       |
|--------------------------|-----------|-------|-------|
| many-body component      | A         | В     | С     |
| one-body                 | -178.60   | 31.46 | -4.02 |
| two-body                 | -0.55     | -0.47 | 0.02  |
| polynomials              | -1.92     | -0.52 | 0.08  |
| dispersion               | -0.03     | 0.09  | -0.11 |
| permanent electrostatics | 1.39      | -0.04 | 0.05  |
| three-body               | 0.05      | 0.42  | -0.06 |
| induced electrostatics   | 1.39      | -0.21 | 0.07  |
| total                    | -177.71   | 31.20 | -3.99 |

this component only contributed 1.39 cm<sup>-1</sup> to this 2-MR anharmonic coupling term.

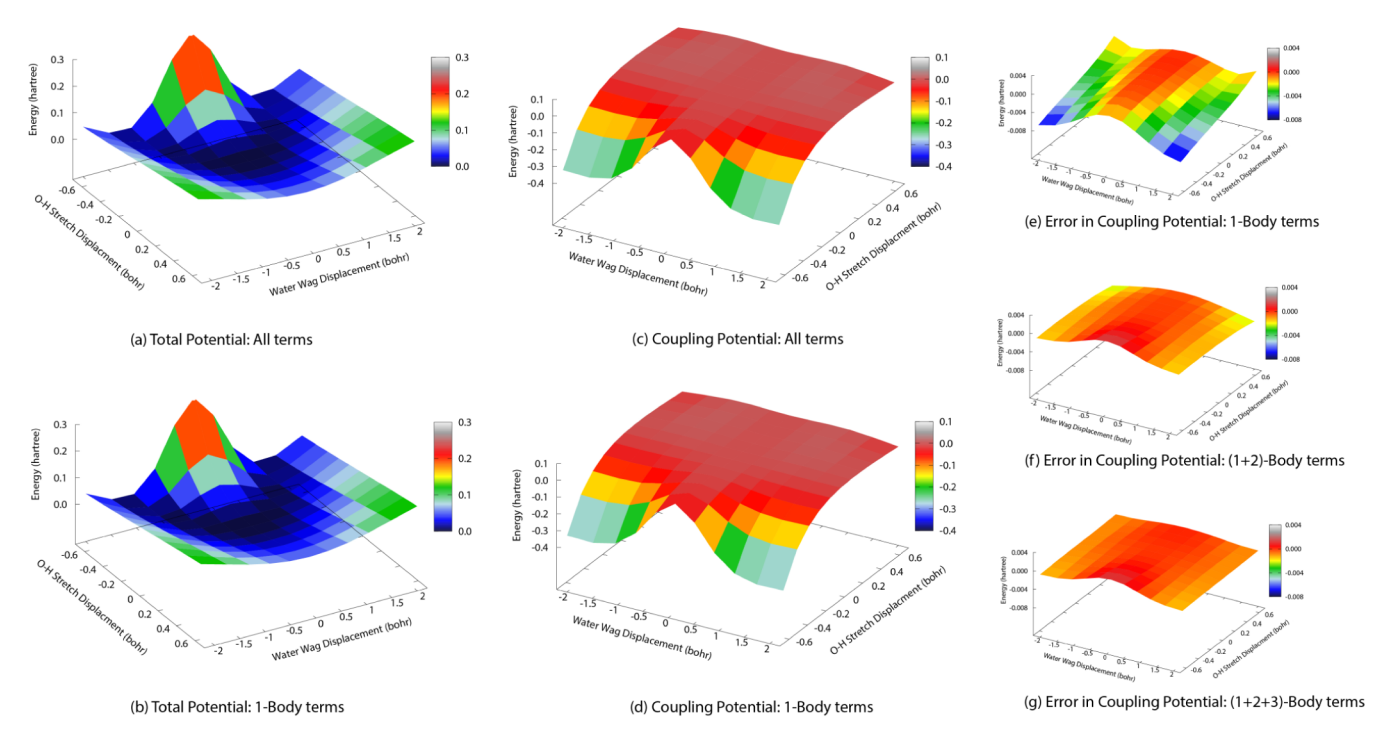


Figure 9. Potential energy surfaces for mode pair A of  $Cs^+(H_2O)_{20}$  of Figure 8. (a)–(b) Total 2-MR vibrational potentials using the full MBX potential and one-body terms only. (c)–(d) 2-MR coupling surfaces  $\Delta V^{(2)}(q_i,q_j)$  using the full MBX potential and one-body terms only. (e)–(g) Coupling potential error surfaces for a series of many-body components, relative to the full coupling potential depicted in panel (c). The orientation in panels (a),(b) differs from the orientation in panels (c)–(g) for visual clarity.

To confirm that this outcome is not specific to certain coupling matrix elements, the potential energy surfaces were directly investigated, and these surfaces-represented on the same quadrature grids used for mode-pair integration—are depicted in Figure 9 for mode pair A. In Figure 9a and b, the total 2-MR PES is presented for the full MBX potential and the one-body terms therein and the surfaces are visually indistinguishable on the admittedly large energy scale of the plots. Clearly, these surfaces are neither the paraboloids that would be expected of 2D harmonic surfaces nor are they simple additions of 1D anharmonic surfaces. As the wag mode is displaced from equilibrium (the origin in these plots), for example, displacement along the O-H stretch considerably changes the potential. These effects are directly probed in the anharmonic coupling surfaces,  $\Delta V^{(2)}(q_{wag},q_{stretch})$ , that are depicted in Figure 9c-d. The scale of the coupling in these panels is similar to the scale of the total potential itself, indicating a strong pairwise interaction between these modes. The one-body representation of this coupling (Figure 9d), however, is again a faithful representation of the two-mode interaction. The error in these coupling surfaces (a  $\Delta\Delta V$  term) is depicted in Figure 9e-g, as a function of many-body truncation order in the MBX potential. The error in the onebody representation of this surface (Figure 9e) is nonzero, but the maximum error across this region of the surface is only about 3% of the total coupling potential. The exponential decay of the vibrational basis functions at the corners of these surfaces further diminishes the role of these deviations and instead emphasizes the small errors near the origin, which leads to the subwavenumber error in the  $C_{00,00}$  coupling value for this mode pair. Addition of two-body contributions (Figure 9f) recovers more than three-quarters of the remnant maximum surface error and more than half of the  $C_{00,00}$  coupling error. Three-body (Figure 9g) and induced-electrostatic contributions remain small and yield nearly flat errors across the potential surface.

Similar behavior was observed for the rock-bend pair (B). Once again, the dominant motions are localized to a common water molecule. Accordingly, one-body terms in the potential contribute 31.46 cm<sup>-1</sup> (100.8%) to the 31.20 cm<sup>-1</sup> total coupling. Two- and three-body terms constitute only -0.47and 0.42 cm<sup>-1</sup>, respectively, with the remnant -0.21 cm<sup>-1</sup> of coupling stemming from the induced-electrostatic terms. Although these many-body terms are critical for the interaction of this water molecule with its hydrogen-bonding partners, as was demonstrated by the harmonic shifts in Figure 2, these cross-monomer effects in the PES mostly cancel in the modepair couplings, leaving mainly one-body contributions to the differential coupling. Both motions partially break a hydrogen bond to the water molecule's H-bond-accepting neighborand break it in different directions—yet the overwhelming majority of this effect is still captured in the one-mode scans and is not borne out in ≥two-body terms of the two-mode anharmonicity. The H-bond-breaking effects are instead captured by the 1-MR anharmonicity, whereas the 2-MR anharmonicity evidently originates only from short-ranged, intramonomer distortion.

The more challenging behavior to explain involved motions that natively included two or more water molecules. Few of these motions are observed in localized coordinate systems, but some certainly still exist in the low-frequency region of vibrational spectra. One example with substantial overall coupling was the dimer-bending motion ( $\tilde{\nu}_{\rm pseudo}$ =172 cm<sup>-1</sup>), depicted in mode pair C of Figure 8. This mode involves the side-to-side displacement of a hydrogen-bond-accepting water monomer, but it also includes the concomitant "following" motion of its hydrogen-bond-donating partner (along with

smaller motions of other water molecules). A hydrogen-bonded O–H stretch ( $\tilde{\nu}_{\rm pseudo}$ = 3602 cm<sup>-1</sup>) constitutes the other member of this modestly coupled mode pair. In this case, one-body terms in the potential contribute –4.02 cm<sup>-1</sup> (100.8%) of the –3.99 cm<sup>-1</sup> total pairwise coupling. Two-body (+0.02 cm<sup>-1</sup>), three-body (–0.06 cm<sup>-1</sup>), and induced-electrostatic (0.07 cm<sup>-1</sup>) components were again observed to be small individually and partially offsetting in aggregate.

If these pair-C motions involve two different water molecules that only interact via two-body (and higher) terms, how could one-body terms still dominate? The answer is essentially geometric in nature. When the dimer bending mode of the "first" water molecule is activated, for example, it reorients and elongates the O-H bond of the "second," Hbond-donating water molecule. Contraction along the O-H stretch mode induces relaxation of this donating water molecule and leads to nonzero coupling. Both of these effects are still dominantly intramonomer relaxation effects, even though they are induced by many-body vibrational motions. The two-body and higher contributions of the potential are critical for holding the cluster together, determining its shape, and—critically—determining its harmonic and 1D anharmonic vibrational motions. But the coupled motion along those modes is still dominantly controlled by geometric distortion of the monomers during pairwise mode displacement, rather than by interwater interaction terms in the many-body potential. Since most of this intramonomer distortion/relaxation is adequately captured by the one-body potential, it naturally also captures the majority of the pairwise vibrational coupling.

Other classes of mode-pair couplings were also examined, including the anharmonic coupling among OH stretches. Although the one-body terms were generally not good representations of these values, the magnitude of such couplings was quite small (<0.1 cm<sup>-1</sup>) and would not meaningfully impact the resulting anharmonic spectra. Across the entire set of OH stretch couplings, the only quantitatively meaningful pairs involved stretches within each water monomer, which are nicely captured by one-body contributions.

Because the preceding analysis was performed in local-mode coordinates, a natural question involves the transferability of these conclusions to other (rectilinear) coordinate systems, such as normal modes. To assess this attribute, the same coupling matrix elements were examined in nonlocal, normalmode coordinates for the same cluster structures. Results are presented in Figures S10 and S11 as direct analogues of Figures 4 and 5 of the main text. In short, all of the same conclusions hold. Although the span of the coupling values necessarily shifts in these alternative coordinates, the one-body dominance remains intact and evidently is not merely an outcome of the localization procedure. An explanation of the local response, based on monomer distortions, is certainly more intuitive in the local displacements, but because normal modes are simply linear combinations of these local displacements (and vice versa), the same underlying physics still applies. The distance dependence depicted in Figure 7 effectively vanishes for normal modes, and this attribute is the main case where the coordinate systems differ. Nonetheless, the major many-body conclusions of this work remain valid in normal-mode coordinates.

**3.5. DFT Comparison.** The transferability of this outcome across potentials was examined with DFT methods for the same three pairs of vibrational modes of  $Cs^+(H_2O)_{20}$ . The

structure exhibited little relaxation upon reoptimization with B97M-V/cc-pVDZ and maintained its overall clathrate-like form. The first two examined pairs of modes exhibited nearly identical atomic displacements with MBX and B97M-V potentials. The wag-stretch pair (A) (348/3894 cm<sup>-1</sup> with MBX and 344/3885 cm<sup>-1</sup> with B97M-V) and the rock-bend pair (B) (463/1654 cm<sup>-1</sup> with MBX and 486/1702 cm<sup>-1</sup> with B97M-V) thus serve as direct comparisons between methods. The best-matched low-frequency motion for the third, dimer bend—stretch combination C contained more heavy-atom stretch component (172/3602 cm<sup>-1</sup> with MBX and 247/3408 cm<sup>-1</sup> with B97M-V) with DFT, but because the same water molecules were involved, it still serves to assess whether many-body contributions behave similarly in this alternative potential. The structure with B97M-V can be found in Section S1.

The values of the total vibrational couplings shifted slightly across methods, but the many-body behavior was nonetheless consistent. The wag-stretch pair (A) exhibited a total coupling of -178.0 cm<sup>-1</sup> (-177.7 cm<sup>-1</sup> with MBX), and one-body contributions comprised -178.3 cm<sup>-1</sup>. Two-body contributions increased the magnitude of this coupling to  $-178.4 \text{ cm}^{-1}$ , leaving only +0.4 cm<sup>-1</sup> as the remnant three-body-and-higher contribution. Similarly, the rock-stretch pair (B) exhibited a total coupling of 26.7 cm<sup>-1</sup> with DFT (31.2 cm<sup>-1</sup> with MBX), of which 26.4 cm<sup>-1</sup> was captured by one-body terms. Addition of two-body terms decreased the coupling to 26.2 cm<sup>-1</sup>, leaving +0.5 cm<sup>-1</sup> as the remnant many-body contribution. For the third mode pair, the somewhat altered low-frequency motion led to a notably smaller pair coupling value of -0.87cm<sup>-1</sup> (-3.99 cm<sup>-1</sup> with MBX). The one-body component is -0.64 cm<sup>-1</sup>, and the summed one- and two-body coupling is -0.82 cm<sup>-1</sup>. In this case, the two-body contribution is relatively larger but still only impacts the coupling by -0.18 cm<sup>-1</sup>. Overall, the dominant one-body behavior of vibrational couplings appears to be retained for quantum chemistry-based fragmentation approaches, with some possibly larger relative deviations for small coupling values. Encouragingly, the spurious role of basis set superposition error (BSSE) in many-body quantum computations 129,147 appears to have largely canceled in these differential quantities, even with the modest double- $\zeta$  basis set employed here—likely because each anharmonicity term involves differences of same-body quantities—but may explain some of the slight, remnant coupling from beyond-two-body terms. We note that portions of polarization and charge-transfer effects, which are the analogues of the induced electrostatics in the MBX potentials, are intrinsically included in the two-body terms in this quantum-focused fragmentation. Whether further refinement of these DFT anharmonicities into constituent contributions (such as permanent electrostatics) could be exploited with energy-decomposition schemes remains an open question for future investigation.

**3.6.** Role in Anharmonic Shifts. Finally, the most obvious open question after examining specific anharmonic coupling terms is the role of these many-body contributions in the ensuing anharmonic spectrum. For the reasons mentioned earlier, full-dimensional anharmonic simulations (VSCF, VCI, etc.) are not viable for a 2-MR representation of the potential for the present ion—water complexes. As a preliminary estimate of these effects, however, two-dimensional eigensolvers were performed for selected strongly coupled mode pairs in Cs<sup>+</sup>(H<sub>2</sub>O)<sub>20</sub> using the MBX potential and its many-body

components. In this analysis, the total many-body 1-MR potential was combined with incremental contributions from each many-body component in the differential 2-MR coupling. This approach does not yet yield the full-dimensional, anharmonic spectrum of the complex, but it does (a) allow for an assessment of each many-body term's contribution to anharmonicity and (b) isolate the role that these many-body components play in shifting the transitions of a specific mode pair. Representative results are listed in Table 2 for the

Table 2. Many-Body Contributions to 2D Anharmonic Fundamental Transitions in  $Cs^+(H_2O)_{20}$ , Using the MBX Potential, for a Hydrogen-Bonded OH Stretch and Water-Wag Vibration Pair

| frequency type | potential  | wag fundamental $(cm^{-1})$ | OH stretch fundamental $(cm^{-1})$ |
|----------------|------------|-----------------------------|------------------------------------|
| harmonic       | total      | 757.9                       | 3593.9                             |
| 1D anharmonic  | total      | 921.0                       | 3383.6                             |
| 2D anharmonic  | one-body   | 728.4                       | 3398.2                             |
|                | two-body   | 736.6                       | 3395.9                             |
|                | three-body | 735.7                       | 3396.5                             |
|                | total      | 733.9                       | 3406.8                             |

fundamental  $(0 \rightarrow 1)$  transitions of a hydrogen-bonded OH stretch and its strongest-coupled mode partner, which, in this case, is a wag motion of the same water molecule. For reference, the  $C_{00,00}$  coupling terms are  $-89.6~{\rm cm}^{-1}$  (total) and  $-92.1~{\rm cm}^{-1}$  (one-body) for this pair; the corresponding  $C_{00,01}$  terms are  $-311.3~{\rm cm}^{-1}$  (total) and  $-310.4~{\rm cm}^{-1}$  (one-body). In this table, two- and three-body entries include preceding many-body terms, and the two-body term includes the sum of permanent electrostatics, dispersion, and polynomial terms.

The results for the total many-body potential in Table 2 indicate that anharmonicity is reasonably strong in this mode pair, with total 2D anharmonic shifts of -24.0 cm<sup>-1</sup> and -187.1 cm<sup>-1</sup> for the wag and stretch, respectively, relative to the local-mode, harmonic pseudofrequencies. Notably, the one-mode anharmonicities are appreciable in these modes, with the 1D wag spuriously shifting 187 cm<sup>-1</sup> to the blue of the 2D anharmonic value (consistent with the results shown in Figure 3). The 1D anharmonic OH stretch shifts the correct direction, by -210.3 cm<sup>-1</sup>, but this value overestimates the true anharmonicity by -23.2 cm<sup>-1</sup>.

The one-body representation of the potential captures the majority of the remnant deviation between the 1D and 2D anharmonicities. In the wag, for example, -192.6 cm<sup>-1</sup> of the -187.1 cm<sup>-1</sup> 2D shift is recovered. In the OH stretch, 14.6 cm<sup>-1</sup> of the 23.2 cm<sup>-1</sup> blue shift is recovered. Some nonmonotonic convergence toward the total 2D value was observed as additional many-body contributions were included, and the induced-electrostatic component (capturing the deviation between the three-body and total entries in Table 2) was found to be nontrivial in this case. These many-body component errors (2-11 cm<sup>-1</sup>) are of the same approximate order of magnitude as the coupling matrix element errors examined throughout this work, so this outcome was reasonably anticipated. A critical caveat, however, is that this analysis likely represents a worst-case scenario because the total potential's contributions to the earlier-discussed bilinear (harmonic) coupling terms are not yet included in the lowerbody potentials. Given the strong sensitivity of the harmonic spectra to beyond-one-body terms in the potential, some

improvement in these results with this future analytic correction is reasonably anticipated.

### 4. CONCLUSION

The many-body contributions to vibrational couplings in clathrate-like, ion—water clusters were shown to primarily originate from one-body contributions to the potential energy surface, even for two-mode couplings. Although the harmonic force constants and single-mode anharmonicities are strongly impacted by two-body (and higher) terms, the differential anharmonic couplings were found to be both short-range and almost entirely one-body in nature. This outcome has potential consequences for both the conceptual understanding of vibrational interactions and their dynamics, as well as spectroscopy simulation methods.

The most obvious methodological route to exploit this behavior would be to use only the one-body terms (and possibly short-range two-body terms, depending on the desired accuracy) when computing spectra with potentials of manybody forms, such as MB-pol for water or MBX for ion-water interactions. Given that the induced electrostatics and threebody polynomials collectively comprise >90% of the computational cost of MBX—and the one-body polynomials constitute <1% of the cost 107—notable computational savings would be accessed by such approximations. Similar low-order screenings could be straightforwardly applied to many-body forms of quantum chemistry potentials (or derivatives thereof for Taylor expansion-based potentials 171,172) that are generated on-the-fly during anharmonic simulations. These natural extensions, of course, only apply in cases where well-defined fragments or related fragmentation schemes are appropriate. An open challenge involves developing means to capture this local electronic response in general molecular systems or systems where the identity of fragments would necessarily be dynamic during the vibrational response.

This outsized influence of short-range, low-order, manybody terms likely helps explain the success of other viewpoints of vibrational motion. For example, the local-monomer  $\mathsf{model}^{173-180}$  is a limiting case of local-mode methods, wherein full-dimensional, variational calculations for individual molecules in a cluster (such as water) are solved in the surrounding, fixed potential of the remaining monomers. If the full cluster potential is able to correctly describe the harmonic and diagonal-anharmonicity response, while the anharmonic coupling accounts for this intramonomer response, it makes sense that this model captures much of the spectral heterogeneity in water clusters. An interesting future investigation would include an analysis of the extent to which this local-monomer anharmonicity is due purely to the monomers' internal electronic response, even in cases where cross-monomer coupling corrections are needed. 120,174 As a second example, several previous studies have demonstrated the success of "multilevel" methods, \$83,154,181-189 wherein terms in the *n*-MR expansion are treated at different levels of theory. The underlying premise of this approach is that important quantum chemistry components, such as electron correlation and basis set effects, cancel in the differential anharmoniccoupling terms. The present analysis's conclusion that onebody effects dominate these couplings may partly explain why such quantum components cancel: Although one-body terms may require spectroscopically accurate potentials, they are invariably short-ranged and require little collective response that would otherwise necessitate long-range correlation and

extended basis sets. And, of course, the short-range, low-order nature of many-body contributions to anharmonic couplings must necessarily be the underlying driving force behind the success of the aforementioned double-incremental expansion. In this case, nearest-neighbor couplings are often sufficient for accurate representations of full 2-MR spectra, and the dominance of intrafragment coupling could reasonably explain such outcomes.

A remnant open question is the generality of these conclusions, which are thus far limited to modestly sized ion—water clusters. Considerable additional testing is needed on hydrated-ion systems with stronger interactions, such as hydrated halides, 190,191 other strongly hydrogen-bonded systems, 38,41,192–197 and cases where covalently linked functional groups define fragments. Given the geometric considerations observed in the present investigation, even in cases of multiwater motions, some degree of transferability to other systems is anticipated. Whether stronger interactions are sufficient to yield strong two-body contributions to anharmonic couplings will nonetheless need to be investigated further. Either way, this new insight into the physics of vibrational couplings potentially opens new avenues for frameworks of vibrational coupling and dynamics.

### ASSOCIATED CONTENT

# Supporting Information

The Supporting Information is available free of charge at https://pubs.acs.org/doi/10.1021/jacs.4c03198.

Cartesian coordinates of optimized structures, ion dependence of harmonic spectra, ion dependence of 1-MR anharmonicities, many-body decomposition of anharmonic couplings, mode-pair animations, and repository of raw coupling and vibrational mode data. Source data is available from the authors upon request (PDF)

Animations of strongly coupled local-mode pairs (ZIP) Cartesian coordinates of optimized structures in xyz files (ZIP)

## AUTHOR INFORMATION

## **Corresponding Author**

Ryan P. Steele – Department of Chemistry and Henry Eyring Center for Theoretical Chemistry, University of Utah, Salt Lake City, Utah 84112, United States; orcid.org/0000-0002-3292-9805; Email: ryan.steele@utah.edu

#### **Authors**

Ryan J. Spencer – Department of Chemistry and Henry Eyring Center for Theoretical Chemistry, University of Utah, Salt Lake City, Utah 84112, United States

Asylbek A. Zhanserkeev – Department of Chemistry and Henry Eyring Center for Theoretical Chemistry, University of Utah, Salt Lake City, Utah 84112, United States

Emily L. Yang — Department of Chemistry and Henry Eyring Center for Theoretical Chemistry, University of Utah, Salt Lake City, Utah 84112, United States; orcid.org/0009-0005-9839-964X

Complete contact information is available at: https://pubs.acs.org/10.1021/jacs.4c03198

## **Author Contributions**

\*R.J.S. and A.A.Z. contributed equally.

#### Notes

The authors declare no competing financial interest.

## ACKNOWLEDGMENTS

The authors acknowledge helpful conversations with Ruihan Zhou and Francesco Paesani concerning the MBX potentials. Funding for this work was provided by the U.S. National Science Foundation under Grant CHE-2102309. The support and resources of the Center for High-Performance Computing at the University of Utah are gratefully acknowledged.

#### REFERENCES

- (1) Bunker, P. R.; Jensen, P. Molecular Symmetry and Spectroscopy; NRC Research Press, 1998.
- (2) Carnegie, P. D.; Marks, J. H.; Brathwaite, A. D.; Ward, T. B.; Duncan, M. A. Microsolvation in  $V^+(H_2O)_n$  Clusters Studied with Selected-Ion Infrared Spectroscopy. *J. Phys. Chem. A* **2020**, 124, 1093–1103.
- (3) Marks, J. H.; Ward, T. B.; Brathwaite, A. D.; Duncan, M. A. Infrared Spectroscopy of Zn(Acetylene)<sub>n</sub><sup>+</sup> Complexes: Ligand Activation and Nascent Polymerization. *J. Phys. Chem. A* **2020**, *124*, 4764–4776.
- (4) Wagner, J. P.; McDonald, D. C.; Colley, J. E.; Franke, P. R.; Duncan, M. A. Infrared Spectroscopy of the Protonated HCl Dimer and Trimer. *J. Chem. Phys.* **2021**, *155*, 134302.
- (5) Batchelor, A. G.; Marks, J. H.; Ward, T. B.; Duncan, M. A.  $Pt^+(C_2H_2)_n$  Complexes Studied with Selected-Ion Infrared Spectroscopy. *J. Phys. Chem. A* **2023**, 127, 5704–5712.
- (6) Sweeney, A. F.; O'Brien, J. T.; Williams, E. R.; Armentrout, P. B. Structural Elucidation of Hydrated CuOH<sup>+</sup> Complexes Using IR Action Spectroscopy and Theoretical Modeling. *Int. J. Mass Spectrom.* **2015**, 378, 270–280.
- (7) Armentrout, P. B.; Stevenson, B. C.; Ghiassee, M.; Boles, G. C.; Berden, G.; Oomens, J. Infrared Multiple-Photon Dissociation Spectroscopy of Cationized Glycine: Effects of Alkali Metal Cation Size on Gas-Phase Conformation. *Phys. Chem. Chem. Phys.* **2022**, 24, 22950–22959.
- (8) Wolk, A. B.; Leavitt, C. M.; Garand, E.; Johnson, M. A. Cryogenic Ion Chemistry and Spectroscopy. *Acc. Chem. Res.* **2014**, *47*, 202–210.
- (9) Talbot, J. J.; Yang, N.; Huang, M.; Duong, C. H.; McCoy, A. B.; Steele, R. P.; Johnson, M. A. Spectroscopic Signatures of Mode-Dependent Tunnel Splitting in the Iodide—Water Binary Complex. J. Phys. Chem. A 2020, 124, 2991—3001.
- (10) Guasco, T. L.; Johnson, M. A.Applications of Lasers and Mass Spectrometry in Molecular Spectroscopy and Molecular Structure Determination In *Emerging Trends In Chemical Applications Of Lasers, Acs Symposium Series*; American Chemical Society: 2021; Vol. 1398; pp. 277306, Doi: .
- (11) Frederiks, N. C.; Hariharan, A.; Johnson, C. J. Spectroscopic Studies of Clusters of Atmospheric Relevance. *Annu. Rev. Phys. Chem.* **2023**, *74*, 99–121.
- (12) Hernández, H. M.; Sun, Q.; Rosati, M.; Gieseking, R. L. M.; Johnson, C. J. Bonding and Acidity of the Formal Hydride in the Prototypical  $\mathrm{Au_9}(\mathrm{PPh_3})_8\mathrm{H_2}^+$  Nanocluster. *Angew. Chem., Int. Ed.* **2023**, *62*, No. e202307723.
- (13) Rizzo, T. R.; Stearns, J. A.; Boyarkin, O. V. Spectroscopic Studies of Cold, Gas-Phase Biomolecular Ions. *Int. Rev. Phys. Chem.* **2009**, *28*, 481–515.
- (14) Pereverzev, A. Y.; Kopysov, V.; Boyarkin, O. V. High Susceptibility of Histidine to Charge Solvation Revealed by Cold Ion Spectroscopy. *Angew. Chem., Int. Ed.* **2017**, *56*, 15639–15643.
- (15) Boyarkin, O. V. Cold Ion Spectroscopy for Structural Identifications of Biomolecules. *Int. Rev. Phys. Chem.* **2018**, *37*, 559–606.
- (16) Pereverzev, A. Y.; Kopysov, V. N.; Boyarkin, O. V. Peptide Bond Ultraviolet Absorption Enables Vibrational Cold-Ion Spectros-

- copy of Nonaromatic Peptides. J. Phys. Chem. Lett. 2018, 9, 5262-5266.
- (17) Solovyeva, E. M.; Pereverzev, A. Y.; Gorshkov, M. V.; Boyarkin, O. V. Ultraviolet Photodissociation of Peptides: New Insight on the Mobile Proton Model. *J. Exp. Theor. Phys.* **2020**, *130*, 626–632.
- (18) Saparbaev, E.; Aladinskaia, V.; Zviagin, A.; Boyarkin, O. V. Microhydration of Biomolecules: Revealing the Native Structures by Cold Ion IR Spectroscopy. *J. Phys. Chem. Lett.* **2021**, *12*, 907–911.
- (19) Zviagin, A.; Kopysov, V.; Nagornova, N. S.; Boyarkin, O. V. Tracking Local and Global Structural Changes in a Protein by Cold Ion Spectroscopy. *Phys. Chem. Chem. Phys.* **2022**, *24*, 8158–8165.
- (20) Keinan, S.; Pines, D.; Kiefer, P. M.; Hynes, J. T.; Pines, E. Solvent-Induced O–H Vibration Red-Shifts of Oxygen-Acids in Hydrogen-Bonded O–H···Base Complexes. *J. Phys. Chem. B* **2015**, 119, 679–692.
- (21) Nesbitt, D. J.; Hynes, J. T. Vibrational Energy Transfer from Highly Excited Anharmonic Oscillators. Dependence on Quantum State and Interaction Potential. *J. Chem. Phys.* **1982**, *76*, 6002–6014.
- (22) Rey, R.; Ingrosso, F.; Elsaesser, T.; Hynes, J. T. Pathways for H<sub>2</sub>O Bend Vibrational Relaxation in Liquid Water. *J. Phys. Chem. A* **2009**, *113*, 8949–8962.
- (23) Rey, R.; Hynes, J. T. Tracking Energy Transfer from Excited to Accepting Modes: Application to Water Bend Vibrational Relaxation. *Phys. Chem. Phys.* **2012**, *14*, 6332–6342.
- (24) Laage, D.; Stirnemann, G.; Hynes, J. T. Water Jump Reorientation and Ultrafast Vibrational Spectroscopy. *J. Photochem. Photobiol.*, A 2012, 234, 75–82.
- (25) Laage, D.; Demirdjian, H.; Hynes, J. T. Intermolecular Vibration–Vibration Energy Transfer in Solution: Hydrogen Fluoride in Water. *Chem. Phys. Lett.* **2005**, 405, 453–458.
- (26) Rey, R.; Møller, K. B.; Hynes, J. T. Ultrafast Vibrational Population Dynamics of Water and Related Systems: A Theoretical Perspective. *Chem. Rev.* **2004**, *104*, 1915–1928.
- (27) Rey, R.; Hynes, J. T. Vibrational Energy Relaxation of HOD in Liquid D<sub>2</sub>O. *J. Chem. Phys.* **1996**, *104*, 2356–2368.
- (28) Klippenstein, S. J.; Hynes, J. T. Direct and Indirect Solvent Coupling Vibrational Dephasing Mechanisms in Hydrogen-Bonded Molecules. *J. Phys. Chem.* **1991**, *95*, 4651–4659.
- (29) Sibert, E. L., III; Reinhardt, W. P.; Hynes, J. T. Intramolecular Vibrational Relaxation and Spectra of CH and CD Overtones in Benzene and Perdeuterobenzene. *J. Chem. Phys.* **1984**, *81*, 1115–1134.
- (30) Yang, D.; Liu, L.; Xie, D.; Guo, H. Full-Dimensional Quantum Studies of Vibrational Energy Transfer Dynamics between H<sub>2</sub>O and Ar: Theory Assessing Experiment. *Phys. Chem. Chem. Phys.* **2022**, *24*, 13542–13549.
- (31) Demirdöven, N.; Khalil, M.; Tokmakoff, A. Correlated Vibrational Dynamics Revealed by Two-Dimensional Infrared Spectroscopy. *Phys. Rev. Lett.* **2002**, *89*, 237401.
- (32) Demirdöven, N.; Khalil, M.; Golonzka, O.; Tokmakoff, A. Correlation Effects in the Two-Dimensional Vibrational Spectroscopy of Coupled Vibrations. *J. Phys. Chem. A* **2001**, *105*, 8025–8030.
- (33) Golonzka, O.; Khalil, M.; Demirdöven, N.; Tokmakoff, A. Coupling and Orientation between Anharmonic Vibrations Characterized with Two-Dimensional Infrared Vibrational Echo Spectroscopy. *J. Chem. Phys.* **2001**, *115*, 10814–10828.
- (34) Petti, M. K.; Lomont, J. P.; Maj, M.; Zanni, M. T. Two-Dimensional Spectroscopy Is Being Used to Address Core Scientific Questions in Biology and Materials Science. *J. Phys. Chem. B* **2018**, 122, 1771–1780.
- (35) Ghosh, A.; Ostrander, J. S.; Zanni, M. T. Watching Proteins Wiggle: Mapping Structures with Two-Dimensional Infrared Spectroscopy. *Chem. Rev.* **2017**, *117*, 10726–10759.
- (36) Johnson, C. L.; Knighton, B. E.; Johnson, J. A. Distinguishing Nonlinear Terahertz Excitation Pathways with Two-Dimensional Spectroscopy. *Phys. Rev. Lett.* **2019**, *122*, 073901.
- (37) McCoy, A. B.; Guasco, T. L.; Leavitt, C. M.; Olesen, S. G.; Johnson, M. A. Vibrational Manifestations of Strong Non-Condon Effects in the  $H_3O^+\cdot X_3$  (X = Ar,  $N_2$ ,  $CH_4$ ,  $H_2O$ ) Complexes: A

- Possible Explanation for the Intensity in the "Association Band" in the Vibrational Spectrum of Water. *Phys. Chem. Chem. Phys.* **2012**, *14*, 7205–7214.
- (38) Duong, C. H.; Yang, N.; Johnson, M. A.; DiRisio, R. J.; McCoy, A. B.; Yu, Q.; Bowman, J. M. Disentangling the Complex Vibrational Mechanics of the Protonated Water Trimer by Rational Control of Its Hydrogen Bonds. *J. Phys. Chem. A* **2019**, *123*, 7965–7972.
- (39) Leavitt, C. M.; Wolk, A. B.; Fournier, J. A.; Kamrath, M. Z.; Garand, E.; Van Stipdonk, M. J.; Johnson, M. A. Isomer-Specific IR—IR Double Resonance Spectroscopy of D<sub>2</sub>-Tagged Protonated Dipeptides Prepared in a Cryogenic Ion Trap. *J. Phys. Chem. Lett.* **2012**, *3*, 1099–1105.
- (40) Yang, N.; Khuu, T.; Mitra, S.; Duong, C. H.; Johnson, M. A.; DiRisio, R. J.; McCoy, A. B.; Miliordos, E.; Xantheas, S. S. Isolating the Contributions of Specific Network Sites to the Diffuse Vibrational Spectrum of Interfacial Water with Isotopomer-Selective Spectroscopy of Cold Clusters. *J. Phys. Chem. A* **2020**, *124*, 10393–10406.
- (41) Zeng, H. J.; Johnson, M. A. Demystifying the Diffuse Vibrational Spectrum of Aqueous Protons through Cold Cluster Spectroscopy. *Annu. Rev. Phys. Chem.* **2021**, *72*, 667–691.
- (42) Polfer, N. C. Infrared Multiple Photon Dissociation Spectroscopy of Trapped Ions. Chem. Soc. Rev. 2011, 40, 2211–2221.
- (43) Garand, E. Spectroscopy of Reactive Complexes and Solvated Clusters: A Bottom-up Approach Using Cryogenic Ion Traps. *J. Phys. Chem. A* **2018**, *122*, 6479–6490.
- (44) Marsh, B. M.; Voss, J. M.; Garand, E. A Dual Cryogenic Ion Trap Spectrometer for the Formation and Characterization of Solvated Ionic Clusters. *J. Chem. Phys.* **2015**, *143*, 204201.
- (45) Martens, J.; Berden, G.; Gebhardt, C. R.; Oomens, J. Infrared Ion Spectroscopy in a Modified Quadrupole Ion Trap Mass Spectrometer at the FELIX Free Electron Laser Laboratory. *Rev. Sci. Instrum.* **2016**, *87*, 103108.
- (46) Vendrell, O.; Gatti, F.; Meyer, H.-D. Dynamics and Infrared Spectroscopy of the Protonated Water Dimer. *Angew. Chem., Int. Ed.* **2007**, *46*, 6918–6921.
- (47) Schröder, M.; Meyer, H.-D. Calculation of the Vibrational Excited States of Malonaldehyde and Their Tunneling Splittings with the Multi-Configuration Time-Dependent Hartree Method. *J. Chem. Phys.* **2014**, *141* (3), 034116.
- (48) Schröder, M.; Gatti, F.; Lauvergnat, D.; Meyer, H.-D.; Vendrell, O. The Coupling of the Hydrated Proton to Its First Solvation Shell. *Nat. Commun.* **2022**, *13*, 6170.
- (49) Carrington, J. T.; Wang, X.-G. Computing Ro-Vibrational Spectra of Van Der Waals Molecules. *WIREs Comput. Mol. Sci.* **2011**, *1* (6), 952–963.
- (50) Carrington, T., Jr Perspective: Computing (Ro-)Vibrational Spectra of Molecules with More Than Four Atoms. *J. Chem. Phys.* **2017**, *146* (12), 120902.
- (51) Felker, P. M.; Bačić, Z. Intermolecular Vibrational States of HF Trimer from Rigorous Nine-Dimensional Quantum Calculations: Strong Coupling between Intermolecular Bending and Stretching Vibrations and the Importance of the Three-Body Interactions. *J. Chem. Phys.* **2022**, *157* (19), 194103.
- (52) Felker, P. M.; Bačić, Z. Noncovalently Bound Molecular Complexes Beyond Diatom—Diatom Systems: Full-Dimensional, Fully Coupled Quantum Calculations of Rovibrational States. *Phys. Chem. Chem. Phys.* **2022**, *24*, 24655–24676.
- (53) Carter, S.; Bowman, J. M.; Handy, N. C. Extensions and Tests of "Multimode": A Code to Obtain Accurate Vibration/Rotation Energies of Many-Mode Molecules. *Theor. Chem. Acc.* **1998**, *100*, 191–198.
- (54) Yu, Q.; Qu, C.; Houston, P. L.; Conte, R.; Nandi, A.; Bowman, J. M. M. the n-Mode Representation of the Potential and Illustrations to IR Spectra of Glycine and Two Protonated Water Clusters. In *Vibrational Dynamics of Molecules*; WORLD SCIENTIFIC, 2021; pp. 296339. Doi: .
- (55) Roy, T. K. Performance of Vibrational Self-Consistent Field Theory for Accurate Potential Energy Surfaces: Fundamentals, Excited States, and Intensities. *J. Phys. Chem. A* **2022**, *126*, 608–622.

- (56) Roy, T. K.; Carrington, T., Jr; Gerber, R. B. Approximate First-Principles Anharmonic Calculations of Polyatomic Spectra Using MP2 and B3LYP Potentials: Comparisons with Experiment. *J. Phys. Chem. A* **2014**, *118*, 6730–6739.
- (57) Sibert, E. L. Modeling Anharmonic Effects in the Vibrational Spectra of High-Frequency Modes. *Annu. Rev. Phys. Chem.* **2023**, *74*, 219–244.
- (58) Carrington, J. T. Using Iterative Methods to Compute Vibrational Spectra *Handbook of High-Resolution Spectroscopy*; John Wiley & Sons, Ltd, 2011, .
- (59) Bowman, J. M. Self-Consistent Field Energies and Wavefunctions for Coupled Oscillators. J. Chem. Phys. 1978, 68, 608-610.
- (60) Christoffel, K. M.; Bowman, J. M. Investigations of Self-Consistent Field, SCF CI and Virtual State Configuration Interaction Vibrational Energies for a Model Three-Mode System. *Chem. Phys. Lett.* **1982**, *85*, 220–224.
- (61) Bowman, J. M. The Self-Consistent-Field Approach to Polyatomic Vibrations. Acc. Chem. Res. 1986, 19, 202-208.
- (62) Wierzbicki, A.; Bowman, J. M. Self-Consistent Field Investigation of Vibrations of Atomic Adsorbates. *J. Chem. Phys.* 1987, 87, 2363–2369.
- (63) Carter, S.; Culik, S. J.; Bowman, J. M. Vibrational Self-Consistent Field Method for Many-Mode Systems: A New Approach and Application to the Vibrations of CO Adsorbed on Cu(100). *J. Chem. Phys.* **1997**, *107*, 10458–10469.
- (64) Hirata, S.; Keçeli, M.; Yagi, K. First-Principles Theories for Anharmonic Lattice Vibrations. J. Chem. Phys. 2010, 133, 034109.
- (65) Keçeli, M.; Hirata, S. Size-Extensive Vibrational Self-Consistent Field Method. *J. Chem. Phys.* **2011**, *135*, 134108.
- (66) Christiansen, O. A Second Quantization Formulation of Multimode Dynamics. *J. Chem. Phys.* **2004**, 120, 2140–2148.
- (67) Christiansen, O. Selected New Developments in Vibrational Structure Theory: Potential Construction and Vibrational Wave Function Calculations. *Phys. Chem. Chem. Phys.* **2012**, *14*, 6672–6687
- (68) Erba, A.; Maul, J.; Ferrabone, M.; Dovesi, R.; Rerat, M.; Carbonniere, P. Anharmonic Vibrational States of Solids from DFT Calculations. Part II: Implementation of the VSCF and VCI Methods. *J. Chem. Theory Comput.* **2019**, *15*, 3766–3777.
- (69) Roy, T. K.; Gerber, R. B. Vibrational Self-Consistent Field Calculations for Spectroscopy of Biological Molecules: New Algorithmic Developments and Applications. *Phys. Chem. Chem. Phys.* **2013**, *15*, 9468–9492.
- (70) Roy, T. K.; Sharma, R.; Gerber, R. B. First-Principles Anharmonic Quantum Calculations for Peptide Spectroscopy: VSCF Calculations and Comparison with Experiments. *Phys. Chem. Chem. Phys.* **2016**, *18*, 1607–1614.
- (71) Gerber, R. B.; Chaban, G. M.; Brauer, B.; Miller, Y. Theory and Applications of Computational Chemistry: The First 40 Years. In Theory and Applications of Computational Chemistry: the First 40 Years; Elsevier, 2005; pp. 165193.
- (72) Jung, J. O.; Gerber, R. B. Vibrational Wave Functions and Spectroscopy of  $(H_2O)_n$ , n=2,3,4,5: Vibrational Self-Consistent Field with Correlation Corrections. *J. Chem. Phys.* **1996**, *105*, 10332–10348
- (73) Matsunaga, N.; Chaban, G. M.; Gerber, R. B. Degenerate Perturbation Theory Corrections for the Vibrational Self-Consistent Field Approximation: Method and Applications. *J. Chem. Phys.* **2002**, *117*, 3541–3547.
- (74) Mathea, T.; Rauhut, G. Advances in Vibrational Configuration Interaction Theory Part 1: Efficient Calculation of Vibrational Angular Momentum Terms. *J. Comput. Chem.* **2021**, *42*, 2321–2333.
- (75) Mathea, T.; Petrenko, T.; Rauhut, G. Advances in Vibrational Configuration Interaction Theory Part 2: Fast Screening of the Correlation Space. *J. Comput. Chem.* **2022**, *43*, 6–18.
- (76) Panek, P. T.; Hoeske, A. A.; Jacob, C. R. On the Choice of Coordinates in Anharmonic Theoretical Vibrational Spectroscopy: Harmonic vs. Anharmonic Coupling in Vibrational Configuration Interaction. *J. Chem. Phys.* **2019**, *150*, 054107.

- (77) Christiansen, O. Vibrational Coupled Cluster Theory. J. Chem. Phys. 2004, 120, 2149–2159.
- (78) Godtliebsen, I. H.; Thomsen, B.; Christiansen, O. Tensor Decomposition and Vibrational Coupled Cluster Theory. *J. Phys. Chem. A* **2013**, *117*, 7267–7279.
- (79) König, C.; Christiansen, O. Automatic determination of important mode-mode correlations in many-mode vibrational wave functions. *J. Chem. Phys.* **2015**, *142* (14), 144115.
- (80) Franke, P. R.; Stanton, J. F.; Douberly, G. E. How to VPT2: Accurate and Intuitive Simulations of CH Stretching Infrared Spectra Using VPT2+K with Large Effective Hamiltonian Resonance Treatments. *J. Phys. Chem. A* **2021**, *125*, 1301–1324.
- (81) Ramakrishnan, R.; Rauhut, G. Semi-Quartic Force Fields Retrieved from Multi-Mode Expansions: Accuracy, Scaling Behavior, and Approximations. *J. Chem. Phys.* **2015**, *142*, 154118.
- (82) Lin, C. Y.; Gilbert, A. T. B.; Gill, P. M. W. Calculating Molecular Vibrational Spectra Beyond the Harmonic Approximation. *Theor. Chem. Acc.* **2008**, *120*, 23–35.
- (83) Yagi, K.; Hirata, S.; Hirao, K. Multiresolution Potential Energy Surfaces for Vibrational State Calculations. *Theor. Chem. Acc.* **2007**, *118*, 681–691.
- (84) Sparta, M.; Høyvik, I.-M.; Toffoli, D.; Christiansen, O. Potential Energy Surfaces for Vibrational Structure Calculations from a Multiresolution Adaptive Density-Guided Approach: Implementation and Test Calculations. *J. Phys. Chem. A* **2009**, *113*, 8712–8723.
- (85) Carter, S.; Bowman, J. M.; Braams, B. J. On Using Low-Order Hermite Interpolation in 'Direct Dynamics' Calculations of Vibrational Energies Using the Code 'Multimode'. *Chem. Phys. Lett.* **2001**, 342, 636–642.
- (86) Carter, S.; Handy, N. C. On the Representation of Potential Energy Surfaces of Polyatomic Molecules in Normal Coordinates. *Chem. Phys. Lett.* **2002**, 352, 1–7.
- (87) Avila, G.; Carrington, T., Jr Solving the Vibrational Schrödinger Equation Using Bases Pruned to Include Strongly Coupled Functions and Compatible Quadratures. *J. Chem. Phys.* **2012**, *137*, 174108.
- (88) Strobusch, D.; Scheurer, C. Adaptive Sparse Grid Expansions of the Vibrational Hamiltonian. J. Chem. Phys. 2014, 140 (7), 074111.
- (89) Sparta, M.; Toffoli, D.; Christiansen, O. An Adaptive Density-Guided Approach for the Generation of Potential Energy Surfaces of Polyatomic Molecules. *Theor. Chem. Acc.* **2009**, *123*, 413–429.
- (90) Babin, V.; Leforestier, C.; Paesani, F. Development of a "First Principles" Water Potential with Flexible Monomers: Dimer Potential Energy Surface, VRT Spectrum, and Second Virial Coefficient. *J. Chem. Theory Comput.* **2013**, *9*, 5395–5403.
- (91) Babin, V.; Medders, G. R.; Paesani, F. Development of a "First Principles" Water Potential with Flexible Monomers. II: Trimer Potential Energy Surface, Third Virial Coefficient, and Small Clusters. *J. Chem. Theory Comput.* **2014**, *10*, 1599–1607.
- (92) Medders, G. R.; Babin, V.; Paesani, F. Development of a "First-Principles" Water Potential with Flexible Monomers. III. Liquid Phase Properties. *J. Chem. Theory Comput.* **2014**, *10*, 2906–2910.
- (93) Medders, G. R.; Paesani, F. Infrared and Raman Spectroscopy of Liquid Water through "First-Principles" Many-Body Molecular Dynamics. *J. Chem. Theory Comput.* **2015**, *11*, 1145–1154.
- (94) Brown, S. E.; Götz, A. W.; Cheng, X.; Steele, R. P.; Mandelshtam, V. A.; Paesani, F. Monitoring Water Clusters "Melt" through Vibrational Spectroscopy. *J. Am. Chem. Soc.* **2017**, *139*, 7082–7088.
- (95) Lambros, E.; Dasgupta, S.; Palos, E.; Swee, S.; Hu, J.; Paesani, F. General Many-Body Framework for Data-Driven Potentials with Arbitrary Quantum Mechanical Accuracy: Water as a Case Study. *J. Chem. Theory Comput.* **2021**, *17*, 5635–5650.
- (96) Bull-Vulpe, E. F.; Riera, M.; Bore, S. L.; Paesani, F. Data-Driven Many-Body Potential Energy Functions for Generic Molecules: Linear Alkanes as a Proof-of-Concept Application. *J. Chem. Theory Comput.* **2023**, *19*, 4494–4509.
- (97) Zhou, R.; Riera, M.; Paesani, F. Toward Data-Driven Many-Body Simulations of Biomolecules in Solution: N-Methyl Acetamide

- as a Proxy for the Protein Backbone. J. Chem. Theory Comput. 2023, 19, 4308-4321.
- (98) Manzhos, S.; Dawes, R.; Carrington, T. Neural Network-Based Approaches for Building High Dimensional and Quantum Dynamics-Friendly Potential Energy Surfaces. *Int. J. Quantum Chem.* **2015**, *115*, 1012–1020.
- (99) Manzhos, S.; Wang, X.; Dawes, R.; Carrington, T. A Nested Molecule-Independent Neural Network Approach for High-Quality Potential Fits. J. Phys. Chem. A 2006, 110, 5295–5304.
- (100) Dawes, R.; Thompson, D. L.; Wagner, A. F.; Minkoff, M. Interpolating Moving Least-Squares Methods for Fitting Potential Energy Surfaces: A Strategy for Efficient Automatic Data Point Placement in High Dimensions. J. Chem. Phys. 2008, 128, 084107.
- (101) Yu, Q.; Qu, C.; Houston, P. L.; Nandi, A.; Pandey, P.; Conte, R.; Bowman, J. M. A Status Report on "Gold Standard" Machine-Learned Potentials for Water. *J. Phys. Chem. Lett.* **2023**, *14*, 8077–8087.
- (102) Braams, B. J.; Bowman, J. M. Permutationally Invariant Potential Energy Surfaces in High Dimensionality. *Int. Rev. Phys. Chem.* **2009**, 28, 577–606.
- (103) Bowman, J. M.; Czakó, G.; Fu, B. High-Dimensional Ab Initio Potential Energy Surfaces for Reaction Dynamics Calculations. *Phys. Chem. Chem. Phys.* **2011**, *13*, 8094–8111.
- (104) Xie, Z.; Bowman, J. M. Permutationally Invariant Polynomial Basis for Molecular Energy Surface Fitting Via Monomial Symmetrization. *J. Chem. Theory Comput.* **2010**, *6*, 26–34.
- (105) Jiang, B.; Li, J.; Guo, H. Potential Energy Surfaces from High Fidelity Fitting of Ab Initio Points: The Permutation Invariant Polynomial Neural Network Approach. *Int. Rev. Phys. Chem.* **2016**, 35, 479–506.
- (106) Jiang, B.; Guo, H. Permutation Invariant Polynomial Neural Network Approach to Fitting Potential Energy Surfaces. *J. Chem. Phys.* **2013**, *139*, 054112.
- (107) Riera, M.; Knight, C.; Bull-Vulpe, E. F.; Zhu, X.; Agnew, H.; Smith, D. G. A.; Simmonett, A. C.; Paesani, F. MBX: A Many-Body Energy and Force Calculator for Data-Driven Many-Body Simulations. *J. Chem. Phys.* **2023**, *159* (5), 054802.
- (108) Cheng, X.; Steele, R. P. Efficient Anharmonic Vibrational Spectroscopy for Large Molecules Using Local-Mode Coordinates. *J. Chem. Phys.* **2014**, *141*, 104105.
- (109) Cheng, X.; Talbot, J. J.; Steele, R. P. Tuning Vibrational Mode Localization with Frequency Windowing. *J. Chem. Phys.* **2016**, *145*, 124112.
- (110) Jacob, C. R.; Reiher, M. Localizing Normal Modes in Large Molecules. J. Chem. Phys. 2009, 130, 084106.
- (111) Neff, M.; Rauhut, G. Toward Large Scale Vibrational Configuration Interaction Calculations. *J. Chem. Phys.* **2009**, *131* (12), 124129.
- (112) Weymuth, T.; Jacob, C. R.; Reiher, M. A Local-Mode Model for Understanding the Dependence of the Extended Amide III Vibrations on Protein Secondary Structure. *J. Phys. Chem. B* **2010**, *114*, 10649–10660.
- (113) Panek, P. T.; Jacob, C. R. Efficient Calculation of Anharmonic Vibrational Spectra of Large Molecules with Localized Modes. *ChemPhyschem.* **2014**, *15*, 3365–3377.
- (114) Panek, P. T.; Jacob, C. R. On the Benefits of Localized Modes in Anharmonic Vibrational Calculations for Small Molecules. *J. Chem. Phys.* **2016**, *144*, 164111.
- (115) Kuenzer, U.; Klotz, M.; Hofer, T. S. Probing Vibrational Coupling Via a Grid-Based Quantum Approach-an Efficient Strategy for Accurate Calculations of Localized Normal Modes in Solid-State Systems. J. Comput. Chem. 2018, 39, 2196–2209.
- (116) Seidler, P.; Kaga, T.; Yagi, K.; Christiansen, O.; Hirao, K. On the Coupling Strength in Potential Energy Surfaces for Vibrational Calculations. *Chem. Phys. Lett.* **2009**, *483*, 138–142.
- (117) König, C.; Christiansen, O. Linear-Scaling Generation of Potential Energy Surfaces Using a Double Incremental Expansion. *J. Chem. Phys.* **2016**, *145*, 064105.

- (118) Madsen, D.; Christiansen, O.; König, C. Anharmonic Vibrational Spectra from Double Incremental Potential Energy and Dipole Surfaces. *Phys. Chem. Chem. Phys.* **2018**, *20*, 3445–3456.
- (119) Paesani, F.; Bajaj, P.; Riera, M. Chemical Accuracy in Modeling Halide Ion Hydration from Many-Body Representations. *Adv. At. Mol. Phys.* **2019**, *4*, 1631212.
- (120) Riera, M.; Talbot, J. J.; Steele, R. P.; Paesani, F. Infrared Signatures of Isomer Selectivity and Symmetry Breaking in the  $Cs^+(H_2O)_3$  Complex Using Many-Body Potential Energy Functions. *J. Chem. Phys.* **2020**, *153*, 044306.
- (121) Heindel, J. P.; Xantheas, S. S. The Many-Body Expansion for Aqueous Systems Revisited: II. Alkali Metal and Halide Ion—Water Interactions. *J. Chem. Theory Comput.* **2021**, *17*, 2200—2216.
- (122) Yanai, K.; Ishimura, K.; Nakayama, A.; Schmidt, M. W.; Gordon, M. S.; Hasegawa, J.-Y. Electronic Polarization Effect of the Water Environment in Charge-Separated Donor—Acceptor Systems: An Effective Fragment Potential Model Study. *J. Phys. Chem. A* **2016**, 120, 10273—10280.
- (123) Heindel, J. P.; Herman, K. M.; Xantheas, S. S. Many-Body Effects in Aqueous Systems: Synergies between Interaction Analysis Techniques and Force Field Development. *Annu. Rev. Phys. Chem.* **2023**, *74*, 337–360.
- (124) Herman, K. M.; Xantheas, S. S. An Extensive Assessment of the Performance of Pairwise and Many-Body Interaction Potentials in Reproducing Ab Initio Benchmark Binding Energies for Water Clusters n = 2–25. *Phys. Chem. Chem. Phys.* **2023**, 25, 7120–7143.
- (125) Heindel, J. P.; Kirov, M. V.; Xantheas, S. S. Hydrogen Bond Arrangements in  $(H_2O)_{20,\ 24,\ 28}$  Clathrate Hydrate Cages: Optimization and Many-Body Analysis. *J. Chem. Phys.* **2022**, *157*, 094301.
- (126) Raghavachari, K.; Saha, A. Accurate Composite and Fragment-Based Quantum Chemical Models for Large Molecules. *Chem. Rev.* **2015**, *115*, 5643–5677.
- (127) Richard, R. M.; Lao, K. U.; Herbert, J. M. Understanding the Many-Body Expansion for Large Systems. I. Precision Considerations. *J. Chem. Phys.* **2014**, *141*, 014108.
- (128) Lao, K. U.; Liu, K.-Y.; Richard, R. M.; Herbert, J. M. Understanding the Many-Body Expansion for Large Systems. II. Accuracy Considerations. *J. Chem. Phys.* **2016**, *144*, 164105.
- (129) Liu, K.-Y.; Herbert, J. M. Understanding the Many-Body Expansion for Large Systems. III. Critical Role of Four-Body Terms, Counterpoise Corrections, and Cutoffs. *J. Chem. Phys.* **2017**, *147*, 161729
- (130) Broderick, D. R.; Herbert, J. M. Scalable Generalized Screening for High-Order Terms in the Many-Body Expansion: Algorithm, Open-Source Implementation, and Demonstration. *J. Chem. Phys.* **2023**, *159*, 174801.
- (131) Liu, K.-Y.; Herbert, J. M. Energy-Screened Many-Body Expansion: A Practical yet Accurate Fragmentation Method for Quantum Chemistry. J. Chem. Theory Comput. 2020, 16, 475–487.
- (132) Sattasathuchana, T.; Xu, P.; Gordon, M. S. An Accurate Quantum-Based Approach to Explicit Solvent Effects: Interfacing the General Effective Fragment Potential Method with Ab Initio Electronic Structure Theory. J. Phys. Chem. A 2019, 123, 8460–8475. (133) Thapa, B.; Beckett, D.; Jovan Jose, K. V.; Raghavachari, K. Assessment of Fragmentation Strategies for Large Proteins Using the
- Assessment of Fragmentation Strategies for Large Proteins Using the Multilayer Molecules-in-Molecules Approach. J. Chem. Theory Comput. 2018, 14, 1383–1394.
- (134) Mayhall, N. J.; Raghavachari, K. Many-Overlapping-Body (MOB) Expansion: A Generalized Many Body Expansion for Nondisjoint Monomers in Molecular Fragmentation Calculations of Covalent Molecules. *J. Chem. Theory Comput.* **2012**, *8*, 2669–2675.
- (135) Liu, J.; Herbert, J. M. Pair—Pair Approximation to the Generalized Many-Body Expansion: An Alternative to the Four-Body Expansion for Ab Initio Prediction of Protein Energetics Via Molecular Fragmentation. J. Chem. Theory Comput. 2016, 12, 572—584
- (136) Gurunathan, P. K.; Acharya, A.; Ghosh, D.; Kosenkov, D.; Kaliman, I.; Shao, Y.; Krylov, A. I.; Slipchenko, L. V. Extension of the

- Effective Fragment Potential Method to Macromolecules. J. Phys. Chem. B 2016, 120, 6562-6574.
- (137) Kim, Y.; Bui, Y.; Tazhigulov, R. N.; Bravaya, K. B.; Slipchenko, L. V. Effective Fragment Potentials for Flexible Molecules: Transferability of Parameters and Amino Acid Database. *J. Chem. Theory Comput.* **2020**, *16*, 7735–7747.
- (138) Slipchenko, L. V.; Gurunathan, P. K. Effective Fragment Potential Method: Past, Present, and Future. *Fragmentation* **2017**, 183208.
- (139) Floris, S. D.; Talbot, J. J.; Wilkinson, M. J.; Herr, J. D.; Steele, R. P. Quantum Molecular Motion in the Mixed Ion-Radical Complex, [(H<sub>2</sub>O)(H<sub>2</sub>S)]+. *Phys. Chem. Chem. Phys.* **2016**, *18*, 27450–27459.
- (140) Talbot, J. J.; Cheng, X.; Herr, J. D.; Steele, R. P. Vibrational Signatures of Electronic Properties in Oxidized Water: Unraveling the Anomalous Spectrum of the Water Dimer Cation. *J. Am. Chem. Soc.* **2016**, *138*, 11936–11945.
- (141) Conte, R.; Qu, C.; Houston, P. L.; Bowman, J. M. Efficient Generation of Permutationally Invariant Potential Energy Surfaces for Large Molecules. *J. Chem. Theory Comput.* **2020**, *16*, 3264–3272.
- (142) Bartlett, R. J.; Musiał, M. Coupled-Cluster Theory in Quantum Chemistry. Rev. Mod. Phys. 2007, 79, 291–352.
- (143) Hill, J. G.; Peterson, K. A. Gaussian basis sets for use in correlated molecular calculations. XI. Pseudopotential-based and allelectron relativistic basis sets for alkali metal (K–Fr) and alkaline earth (Ca–Ra) elements. *J. Chem. Phys.* **2017**, *147* (24), 244106.
- (144) Lim, I. S.; Schwerdtfeger, P.; Metz, B.; Stoll, H. All-Electron and Relativistic Pseudopotential Studies for the Group 1 Element Polarizabilities from K to Element 119. *J. Chem. Phys.* **2005**, *122*, 104103.
- (145) Kendall, R. A.; Dunning, T. H.; Harrison, R. J. Electron Affinities of the First-Row Atoms Revisited. Systematic Basis Sets and Wave Functions. *J. Chem. Phys.* **1992**, *96* (9), 6796–6806.
- (146) Richard, R. M.; Lao, K. U.; Herbert, J. M. Approaching the Complete-Basis Limit with a Truncated Many-Body Expansion. *J. Chem. Phys.* **2013**, 139 (22), 224102.
- (147) Richard, R. M.; Lao, K. U.; Herbert, J. M. Aiming for Benchmark Accuracy with the Many-Body Expansion. *Acc. Chem. Res.* **2014**, *47*, 2828–2836.
- (148) Heindel, J. P.; Xantheas, S. S. The Many-Body Expansion for Aqueous Systems Revisited: I. Water—Water Interactions. *J. Chem. Theory Comput.* **2020**, *16*, 6843—6855.
- (149) Mato, J.; Tzeli, D.; Xantheas, S. S. The Many-Body Expansion for Metals. I. The Alkaline Earth Metals Be, Mg, and Ca. J. Chem. Phys. 2022, 157 (8), 084313.
- (150) König, C.; Hansen, M. B.; Godtliebsen, I. H.; Christiansen, O. FALCON: A Method for Flexible Adaptation of Local Coordinates of Nuclei. *J. Chem. Phys.* **2016**, *144*, 074108.
- (151) MBX; 2024. https://github.com/paesanilab/MBX (accessed 01 August 2023).
- (152) Yang, E. L.; Talbot, J. J.; Spencer, R. J.; Steele, R. P. Pitfalls in the n-Mode Representation of Vibrational Potentials. *J. Chem. Phys.* **2023**, *159*, 204104.
- (153) Steen, N. M.; Byrne, G. D.; Gelbard, E. M. Gaussian Quadratures for the Integrals  $Exp(-X^2)F(X)$ . *Math. Comput.* **1969**, 23, 661–671.
- (154) Zhanserkeev, A. A.; Yang, E. L.; Steele, R. P. Accelerating Anharmonic Spectroscopy Simulations Via Local-Mode, Multilevel Methods. *J. Chem. Theory Comput.H* **2023**, *19*, 5572–5585.
- (155) Mardirossian, N.; Head-Gordon, M. Mapping the Genome of Meta-Generalized Gradient Approximation Density Functionals: The Search for B97M-V. J. Chem. Phys. 2015, 142, 074111.
- (156) Dasgupta, S.; Herbert, J. M. Standard Grids for High-Precision Integration of Modern Density Functionals: SG-2 and SG-3. *J. Comput. Chem.* **2017**, *38*, 869–882.
- (157) Hill, G. ccRepo: A Correlation-Consistent Basis Set Repository. http://www.grant-hill.group.shef.ac.uk/ccrepo/ (accessed 4/15/2024).
- (158) Epifanovsky, E.; Gilbert, A. T. B.; Feng, X.; Lee, J.; Mao, Y.; Mardirossian, N.; Pokhilko, P.; White, A. F.; Coons, M. P.;

- Dempwolff, A. L. Software for the Frontiers of Quantum Chemistry: An Overview of Developments in the Q-Chem 5 Package. *J. Chem. Phys.* **2021**, *155*, 084801.
- (159) Weinhold, F.; Klein, R. A. What Is a Hydrogen Bond? Resonance Covalency in the Supramolecular Domain. *Chem. Educ. Res. Pract.* **2014**, *15*, 276–285.
- (160) Wright, D.; Sangtarash, S.; Mueller, N. S.; Lin, Q.; Sadeghi, H.; Baumberg, J. J. Vibrational Stark Effects: Ionic Influence on Local Fields. *J. Phys. Chem. Lett.* **2022**, *13*, 4905–4911.
- (161) Hush, N. S.; Reimers, J. R. Vibrational Stark Spectroscopy. 1. Basic Theory and Application to the CO Stretch. *J. Phys. Chem.* **1995**, 99, 15798–15805.
- (162) Shin, S.; Kang, H.; Cho, D.; Lee, J. Y.; Kang, H. Effect of Electric Field on Condensed-Phase Molecular Systems. II. Stark Effect on the Hydroxyl Stretch Vibration of Ice. *J. Phys. Chem. C* **2015**, *119*, 15596–15603.
- (163) Hanson-Heine, M. W. D. Examining the Impact of Harmonic Correlation on Vibrational Frequencies Calculated in Localized Coordinates. *J. Chem. Phys.* **2015**, *143* (16), 164104.
- (164) Chapuisat, X.; Iung, C. Vector Parametrization of the N-Body Problem in Quantum Mechanics: Polyspherical Coordinates. *Phys. Rev. A* **1992**, *45*, 6217–6235.
- (165) Gatti, F.; Muñoz, C.; Iung, C. A General Expression of the Exact Kinetic Energy Operator in Polyspherical Coordinates. *J. Chem. Phys.* **2001**, *114*, 8275–8281.
- (166) Iung, C.; Gatti, F. Polyspherical Parametrization of an N-Atom System: Principles and Applications. *Int. J. Quantum Chem.* **2006**, *106*, 130–151.
- (167) Gatti, F.; Iung, C. Exact and Constrained Kinetic Energy Operators for Polyatomic Molecules: The Polyspherical Approach. *Phys. Rep.* **2009**, 484, 1–69.
- (168) Sadri, K.; Lauvergnat, D.; Gatti, F.; Meyer, H.-D. Numeric Kinetic Energy Operators for Molecules in Polyspherical Coordinates. *J. Chem. Phys.* **2012**, *136* (23), 234112.
- (169) Klinting, E. L.; Lauvergnat, D.; Christiansen, O. Vibrational Coupled Cluster Computations in Polyspherical Coordinates with the Exact Analytical Kinetic Energy Operator. *J. Chem. Theory Comput.* **2020**, *16*, 4505–4520.
- (170) Khaliullin, R. Z.; Cobar, E. A.; Lochan, R. C.; Bell, A. T.; Head-Gordon, M. Unravelling the Origin of Intermolecular Interactions Using Absolutely Localized Molecular Orbitals. *J. Phys. Chem. A* **2007**, *111*, 8753–8765.
- (171) Yagi, K.; Hirao, K.; Taketsugu, T.; Schmidt, M. W.; Gordon, M. S. Ab Initio Vibrational State Calculations with a Quartic Force Field: Applications to  $\rm H_2CO$ ,  $\rm C_2H_4$ ,  $\rm CH_3OH$ ,  $\rm CH_3CCH$ , and  $\rm C_6H_6$ . *J. Chem. Phys.* **2004**, *121*, 1383–1389.
- (172) Westbrook, B. R.; Fortenberry, R. C. pbqff: Push-Button Quartic Force Fields. *J. Chem. Theory Comput.* **2023**, *19*, 2606–2615.
- (173) Wang, Y.; Bowman, J. M. Ab Initio Potential and Dipole Moment Surfaces for Water. II. Local-Monomer Calculations of the Infrared Spectra of Water Clusters. J. Chem. Phys. 2011, 134, 154510.
- (174) Wang, Y.; Bowman, J. M. Coupled-Monomers in Molecular Assemblies: Theory and Application to the Water Tetramer, Pentamer, and Ring Hexamer. J. Chem. Phys. 2012, 136, 144113.
- (175) Wang, Y.; Bowman, J. M. IR Spectra of the Water Hexamer: Theory, with Inclusion of the Monomer Bend Overtone, and Experiment Are in Agreement. *J. Phys. Chem. Lett.* **2013**, *4*, 1104–1108.
- (176) Mancini, J. S.; Bowman, J. M. On-the-Fly Ab Intito Calculations of Anharmonic Vibrational Frequencies: Local-Monomer Theory and Application to HCl Clusters. *J. Chem. Phys.* **2013**, *139*, 164115.
- (177) Liu, H.; Wang, Y.; Bowman, J. M. Local-Monomer Calculations of the Intramolecular IR Spectra of the Cage and Prism Isomers of  $HOD(D_2O)_5$  and HOD and  $D_2O$  Ice Ih. *J. Phys. Chem. B* **2014**, *118*, 14124–14131.
- (178) Yu, Q.; Bowman, J. M. Vibrational Second-Order Perturbation Theory (VPT2) Using Local Monomer Normal Modes. *Mol. Phys.* **2015**, *113*, 3964–3971.

- (179) Qu, C.; Bowman, J. M. Ab Initio, Embedded Local-Monomer Calculations of Methane Vibrational Energies in Clathrate Hydrates. *J. Phys. Chem. C* **2016**, *120*, 3167–3175.
- (180) Liu, H.; Wang, Y.; Bowman, J. M. Quantum Local Monomer IR Spectrum of Liquid  $D_2O$  at 300 K from 0 to 4000 cm<sup>-1</sup> Is in near-Quantitative Agreement with Experiment. *J. Phys. Chem. B* **2016**, 120, 2824–2828.
- (181) Benoit, D. M. Fast Vibrational Self-Consistent Field Calculations through a Reduced Mode–Mode Coupling Scheme. *J. Chem. Phys.* **2004**, *120*, 562–573.
- (182) Bounouar, M.; Scheurer, C. Reducing the Vibrational Coupling Network in N-Methylacetamide as a Model for Ab Initio Infrared Spectra Computations of Peptides. *Chem. Phys.* **2006**, 323, 87–101.
- (183) Boese, A. D.; Martin, J. M. L. Vibrational Spectra of the Azabenzenes Revisited: Anharmonic Force Fields. *J. Phys. Chem. A* **2004**, *108*, 3085–3096.
- (184) Begue, D.; Carbonniere, P.; Pouchan, C. Calculations of Vibrational Energy Levels by Using a Hybrid Ab Initio and DFT Quartic Force Field: Application to Acetonitrile. *J. Phys. Chem. A* **2005**, *109*, 4611–4616.
- (185) Rauhut, G. Efficient Calculation of Potential Energy Surfaces for the Generation of Vibrational Wave Functions. *J. Chem. Phys.* **2004**, *121*, 9313–9322.
- (186) Pflüger, K.; Paulus, M.; Jagiella, S.; Burkert, T.; Rauhut, G. Multi-Level Vibrational SCF Calculations and FTIR Measurements on Furazan. *Theor. Chem. Acc.* **2005**, *114*, 327–332.
- (187) Bürger, H.; Kuna, R.; Ma, S.; Breidung, J.; Thiel, W. The Vibrational Spectra of Krypton and Xenon Difluoride: High-Resolution Infrared Studies and Ab Initio Calculations. *J. Chem. Phys.* **1994**, *101*, 1–14.
- (188) Tan, J. A.; Kuo, J.-L. Multilevel Approach for Direct VSCF/VCI Multimode Calculations with Applications to Large "Zundel" Cations. J. Chem. Theory Comput.H 2018, 14, 6405–6416.
- (189) König, C. Tailored Multilevel Approaches in Vibrational Structure Theory: A Route to Quantum Mechanical Vibrational Spectra for Complex Systems. *Int. J. Quantum Chem.* **2020**, *121*, No. e26375.
- (190) Roscioli, J. R.; Diken, E. G.; Johnson, M. A.; Horvath, S.; McCoy, A. B. Prying Apart a Water Molecule with Anionic H-Bonding: A Comparative Spectroscopic Study of the X<sup>-</sup>·H<sub>2</sub>O (X = OH, O, F, Cl, and Br) Binary Complexes in the 600–3800 cm<sup>-1</sup> Region. *J. Phys. Chem. A* **2006**, *110*, 4943–4952.
- (191) Bajaj, P.; Riera, M.; Lin, J. K.; Mendoza Montijo, Y. E.; Gazca, J.; Paesani, F. Halide Ion Microhydration: Structure, Energetics, and Spectroscopy of Small Halide–Water Clusters. *J. Phys. Chem. A* **2019**, 123, 2843–2852.
- (192) Marsh, B. M.; Voss, J. M.; Zhou, J.; Garand, E. Coordination Structure and Charge Transfer in Microsolvated Transition Metal Hydroxide Clusters [MOH]<sup>+</sup>(H<sub>2</sub>O)<sub>1-4</sub>. *Phys. Chem. Chem. Phys.* **2015**, *17*, 23195–23206.
- (193) Thomas, D. A.; Marianski, M.; Mucha, E.; Meijer, G.; Johnson, M. A.; von Helden, G. Ground-State Structure of the Proton-Bound Formate Dimer by Cold-Ion Infrared Action Spectroscopy. *Angew. Chem., Int. Ed.* **2018**, *57*, 10615–10619.
- (194) Khuu, T.; Schleif, T.; Mohamed, A.; Mitra, S.; Johnson, M. A.; Valdiviezo, J.; Heindel, J. P.; Head-Gordon, T. Intra-Cluster Charge Migration Upon Hydration of Protonated Formic Acid Revealed by Anharmonic Analysis of Cold Ion Vibrational Spectra. *J. Phys. Chem.* A 2023, 127, 7501–7509.
- (195) Yang, B.; Rodgers, M. T. Base-Pairing Energies of Proton-Bound Heterodimers of Cytosine and Modified Cytosines: Implications for the Stability of DNA I-Motif Conformations. *J. Am. Chem. Soc.* **2014**, *136*, 282–290.
- (196) Yang, B.; Wu, R. R.; Berden, G.; Oomens, J.; Rodgers, M. T. Infrared Multiple Photon Dissociation Action Spectroscopy of Proton-Bound Dimers of Cytosine and Modified Cytosines: Effects of Modifications on Gas-Phase Conformations. *J. Phys. Chem. B* **2013**, 117, 14191–14201.

(197) McNary, C. P.; Demireva, M.; Martens, J.; Berden, G.; Oomens, J.; Hamlow, L. A.; Rodgers, M. T.; Armentrout, P. B. Infrared Multiple Photon Dissociation Action Spectroscopy of Protonated Unsymmetrical Dimethylhydrazine and Proton-Bound Dimers of Hydrazine and Unsymmetrical Dimethylhydrazine. *Phys. Chem. Chem. Phys.* **2021**, 23, 25877–25885.